

CERN-TH.7419/94  
hep-ph/9410258

# Three-jet production at LEP and the bottom quark mass

**Mikhail Bilenky**<sup>\*)</sup>

DESY-IfH, Platanenallee 6, 15738 Zeuthen, Germany

**Germán Rodrigo**

Dept. de Física Teòrica, Univ. de València,  
E-46100 Burjassot (València), Spain

and

**Arcadi Santamaria**<sup>\*\*)</sup>

TH Division, CERN, 1211 Genève 23, Switzerland

## Abstract

We consider the possibility of extracting the bottom quark mass from LEP data. The inclusive decay rate for  $Z \rightarrow b\bar{b} + \dots$  is obtained at order  $\alpha_s$  by summing up the one-loop two-parton decay rate to the tree-level three-parton rate. We calculate the decay width of the  $Z$ -boson into two and three jets containing the  $b$ -quark including complete quark mass effects. In particular, we give analytic results for a slight modification of the JADE clustering algorithm. We also study the angular distribution with respect to the angle formed between the gluon and the quark jets, which has a strong dependence on the quark mass. The impact of higher order QCD corrections on these observables is briefly discussed. Finally, we present numerical results for some popular jet-clustering algorithms and show that, indeed, these three-jet observables are very sensitive to the  $b$ -quark mass and well suited for its determination at LEP.

CERN-TH.7419/94

September 25, 2013

---

<sup>\*)</sup> On leave of absence from the Joint Institute for Nuclear Research, Dubna, Russia.

<sup>\*\*)</sup>  On leave of absence from Departament de Física Teòrica, Universitat de València, and IFIC, València, Spain.

# 1 Introduction

In the Standard Model of electroweak interactions all fermion masses are free parameters and their origin, although linked to the spontaneous symmetry breaking mechanism, remains secret. Masses of charged leptons are well measured experimentally and neutrino masses, if they exist, are also bounded. In the case of quarks the situation is more complicated because free quarks are not observed in nature. Therefore, one can only get some indirect information on the values of the quark masses. For light quarks ( $m_q < 1$  GeV, the scale at which QCD interactions become strong), that is, for  $u$ -,  $d$ - and  $s$ -quarks, one can define the quark masses as the parameters of the Lagrangian that break explicitly the chiral symmetry of the massless QCD Lagrangian. Then, these masses can be extracted from a careful analysis of meson spectra and meson decay constants. For heavy quarks ( $c$ - and  $b$ -quarks) one can obtain the quark masses from the known spectra of the hadronic bound states by using, e.g., QCD sum rules or lattice calculations. However, since the strong gauge coupling constant is still large at the scale of heavy quark masses, these calculations are plagued by uncertainties and nonperturbative effects.

It would be very interesting to have some experimental information on the quark masses obtained at much larger scales where a perturbative quark mass definition can be used and, presumably, non-perturbative effects are negligible. The measurements at LEP will combine this requirement with very high experimental statistics.

The effects of quark masses can be neglected for many observables in LEP studies, as usually quark masses appear in the ratio  $m_q^2/m_Z^2$ . For the bottom quark, the heaviest quark produced at LEP, and taking a  $b$ -quark mass of about 5 GeV this ratio is 0.003, even if the coefficient in front is 10 we get a correction of about 3%. Effects of this order are measurable at LEP, however, as we will see later, in many cases the actual mass that should be used in the calculations is the *running* mass of the  $b$ -quark computed at the  $m_Z$  scale:  $\bar{m}_b(m_Z) \approx 3$  GeV rendering the effect below the LEP precision for most of the observables.

While this argument is correct for total cross sections for production of  $b$ -quarks it is not completely true for quantities that depend on other variables. In particular it is not true for jet cross sections which depend on a new variable,  $y_c$  (the jet-resolution parameter that defines the jet multiplicity) and which introduces a new scale in the analysis,  $E_c = m_Z \sqrt{y_c}$ . Then, for small values of  $y_c$  there could be contributions coming like  $m_b^2/E_c^2 = (m_b/m_Z)^2/y_c$  which could enhance the mass effect considerably. In addition mass effects could also be enhanced by logarithms of the mass. For instance, the ratio of the phase space for two massive quarks and a gluon to the phase space for three massless particles is  $1 + 8(m_q/m_Z)^2 \log(m_q/m_Z)$ . This represents a 7% effect for  $m_q = 5$  GeV and a 3% effect for  $m_q = 3$  GeV.

The high precision achieved at LEP makes these effects relevant. In fact, they have to be taken into account in the test of the flavour independence of  $\alpha_s(m_Z)$  [1–5]. In particular it has been shown [6] that the biggest systematic error in the measurement of  $\alpha_s^b(m_Z)$  ( $\alpha_s$  obtained from  $b\bar{b}$ -production at LEP from the ratio of three to two jets) comes from the uncertainties in the estimate of the quark mass effects. This in turn means that mass effects have already been seen. Now one can reverse the question and ask about the possibility of measuring the mass of the bottom quark,  $m_b$ , at LEP by assuming the flavour universality of the strong interactions.

Such a measurement will also allow to check the running of  $\bar{m}_b(\mu)$  from  $\mu = m_b$  to  $\mu = m_Z$  as has been done before for  $\alpha_s(\mu)$ . In addition  $\bar{m}_b(m_Z)$  is the crucial input parameter in the analysis of the unification of Yukawa couplings predicted by many grand unified theories and which has attracted much attention in the last years [7].

The importance of quark mass effects in  $Z$ -boson decays has already been discussed in the literature [8]. The complete order  $\alpha_s$  results for the inclusive decay rate of  $Z \rightarrow b\bar{b} + b\bar{b}g + \dots$  can

be found<sup>1</sup> in [9]. The leading quark mass effects for the inclusive  $Z$ -width are known to order  $\alpha_s^3$  for the vector part [11] and to order  $\alpha_s^2$  for the axial-vector part [12]. Quark mass effects for three-jet final states in the process  $e^+e^- \rightarrow q\bar{q}g$  were considered first in [13] for the photonic channel and extended later to the  $Z$  channel in [14] and [15]. Recently [16] calculations of the three-jet event rates, including mass effects, were done for the most popular jet clustering algorithms using the Monte Carlo approach.

In this paper we will discuss the possibility of measuring the  $b$ -quark mass at LEP, in particular, we study bottom quark mass effects in  $Z$  decays into two and three jets. In section 2 we calculate the inclusive decay rate  $Z \rightarrow b\bar{b} + b\bar{b}g + \dots$  at order  $\alpha_s$  by summing one-loop virtual corrections to  $Z \rightarrow b\bar{b}$  and the real gluon bremsstrahlung contribution. Dimensional continuation is used to regularize both infrared (IR) and ultraviolet (UV) divergences. Phase space integrations are also done in  $D$  dimensions. This calculation allows us to understand the details of the cancellation of IR divergences and how some, potentially large, logarithms of the quark mass are absorbed in the running quark mass  $\bar{m}_b(m_Z)$ . In section 3 we calculate analytically the two and three-jet event rates in terms of the jet-resolution parameter  $y_c$  and the mass of the quark for a slight modification of the well-known JADE algorithm [17] suitable for analytic calculations with massive quarks. We also present numerical results for this scheme and for some of the most popular jet-clustering algorithms (DURHAM ( $K_T$ ), JADE and E), estimate higher order contributions and compare with experimental results obtained by the DELPHI Collaboration [2] for 1990-1991 data. If the gluon jet can be identified with good efficiency a very interesting observable, which strongly depends on the quark mass, is the angular distribution with respect to the angle formed between the quark and the gluon jets. This distribution is calculated for massless quarks in section 4: analytically for JADE-type algorithms and numerically for the DURHAM algorithm. We also compute numerically the ratio of massive to massless angular distributions for the four jet-clustering algorithms. In section 5 we summarize the results obtained in the paper and comment on the possibility of using them to measure the  $b$ -quark mass in LEP experiments. Finally in the four appendices we collect all the functions and formulae needed in the body of the paper.

## 2 The inclusive decay rate $Z \rightarrow b\bar{b}$

The main purpose of this paper is to investigate  $b$ -quark mass effects in  $Z$  decays into two and three jets. Since at order  $\alpha_s$  the inclusive decay rate  $Z \rightarrow b\bar{b} + \dots$  is given by the sum of the two- and three-jet decay widths we will start by studying this quantity.

To calculate the total decay rate to order  $\alpha_s$  one has to sum up the virtual one-loop gluonic corrections to the  $Z \rightarrow b\bar{b}$  with the real gluon bremsstrahlung. Both contributions are separately infrared divergent for massless gluons, therefore, some regularization method for the IR divergences is needed. The sum is, however, IR finite.

Since there are many subtleties in this calculation, we sketch it in this section. Both processes,  $Z \rightarrow b\bar{b}$  at one loop and  $Z \rightarrow b\bar{b}g$ , are calculated in arbitrary dimension  $D = 4 - 2\epsilon$  and dimensional regularization is used to regularize the IR divergences [18]. At order  $\alpha_s$  and for massive quarks all IR divergences appear as simple poles  $1/\epsilon$ . We show how the divergences cancel in the sum and obtain the total inclusive rate.

The first step is to compute the decay width  $Z \rightarrow b\bar{b}$  at tree-level in dimension  $D$ . Since there are no IR divergences in this case it is not necessary to do the calculations in arbitrary

---

<sup>1</sup>The order  $\alpha_s$  corrections to the vector part, including the complete mass dependences, were already known from QED calculations [10].

space-time dimensions. However, there are IR divergences at the one-loop level and  $\epsilon$  factors could lead to finite contributions when multiplied by the divergent terms.

The amplitude for the decay  $Z \rightarrow b\bar{b}$  in  $D$  dimensions is

$$T_b^{(0)} = \mu^\epsilon \frac{g}{4c_W} \bar{u}_1 \gamma_\mu (g_V + g_A \gamma_5) v_2 \epsilon^\mu(q), \quad (2.1)$$

where the factor  $\mu^\epsilon$  has been included to make the gauge weak coupling  $g$  dimensionless in  $D$  dimensions;  $u_1$  and  $v_2$  are short-hand notations for the quark (antiquark) spinors,  $u_1 = u(p_1)$  and  $v_2 = v(p_2)$ ,  $\epsilon^\mu(q)$  stands for the polarization vector of the  $Z$ -boson and  $g_V$  ( $g_A$ ) are the vector (axial-vector) neutral current couplings of the quarks in the Standard Model. At tree level and for the  $b$ -quark we have

$$g_V = -1 + \frac{4}{3}s_W^2, \quad g_A = 1. \quad (2.2)$$

Here we denote by  $c_W$  and  $s_W$  the cosine and the sine of the weak mixing angle.

Taking the square of the amplitude, averaging over initial state polarizations, summing over final state polarizations, and adding the phase space factor for the two-body decay given in appendix A [18] we obtain the following decay width in  $D$  dimensions,

$$\Gamma_b^{(0)} = C_b A_b \beta^{1-2\epsilon}, \quad (2.3)$$

with

$$C_b = m_Z \frac{g^2}{c_W^2 64\pi} \frac{\Gamma(1-\epsilon)}{\Gamma(2-2\epsilon)} \left( \frac{m_Z^2}{4\pi\mu^2} \right)^{-\epsilon}, \quad (2.4)$$

and

$$A_b = \frac{1}{2}(3 - \beta^2 - 2\epsilon)g_V^2 + \beta^2(1 - \epsilon)g_A^2. \quad (2.5)$$

In these expressions  $\beta$  is the relative velocity of the produced quarks

$$\beta = \sqrt{1 - 4r_b}, \quad r_b = \frac{m_b^2}{m_Z^2}. \quad (2.6)$$

At the one-loop level (see diagrams in fig. 1b), and after renormalization of the UV divergences<sup>2</sup>, the amplitude can be conveniently parameterized in terms of three form factors,  $f_V$ ,  $f_A$  and  $f_T$ ,

$$T_b = \mu^\epsilon \frac{g}{4c_W} \bar{u}_1 \left( g_V \left( \left( 1 + \frac{1}{2}C_g f_V \right) \gamma_\mu + i \frac{1}{2}C_g f_T \frac{\sigma_{\mu\nu} q^\nu}{2m_b} \right) + g_A \left( 1 + \frac{1}{2}C_g f_A \right) \gamma_\mu \gamma_5 \right) v_2 \epsilon^\mu(q), \quad (2.7)$$

where  $C_g$  is defined as follows,

$$C_g = \frac{\alpha_s}{\pi} \left( \frac{m_Z^2}{4\pi\mu^2} \right)^{-\epsilon} \frac{1}{\Gamma(1-\epsilon)}. \quad (2.8)$$

Here and below we will conventionally use  $\alpha_s = \alpha_s(m_Z)$  to denote the value of the running strong coupling at the  $m_Z$ -scale.

---

<sup>2</sup>Note that conserved currents or partially conserved currents as the vector and axial currents do not get renormalized. Therefore, all UV divergences cancel when one sums properly self-energy and vertex diagrams. The remaining poles in  $\epsilon$  correspond to IR divergences. One can see this by separating carefully the poles corresponding to UV divergences from the poles corresponding to IR divergences.

The form factors,  $f_V$ ,  $f_A$  and  $f_T$ , are related by

$$f_V = f_A + f_T . \quad (2.9)$$

The two functions,  $f_V$  and  $f_A$ , contain an IR divergence, while  $f_T$  is finite. Separating the divergent parts, we can rewrite the real parts of the form factors as follows (at order  $\alpha_s$  the imaginary parts will not contribute)

$$\text{Re} \{f_V\} = -\frac{1}{\epsilon} f_\epsilon + f_{Vf} , \quad (2.10)$$

$$\text{Re} \{f_A\} = -\frac{1}{\epsilon} f_\epsilon + f_{Af} , \quad (2.11)$$

$$\text{Re} \{f_T\} \equiv f_{Tf} , \quad (2.12)$$

where all functions  $f_\epsilon$ ,  $f_{Vf}$ ,  $f_{Af}$  and  $f_{Tf}$  are given in appendix B. Note that, as expected, the IR divergent part of the amplitude is proportional to the tree-level amplitude eq. (2.1). As the IR divergence manifests itself as a single pole in  $\epsilon$ , clearly, we only need to keep everywhere terms linear in  $\epsilon$ .

From the amplitude (2.7) we obtain the one-loop corrected width in  $D$  dimensions

$$\Gamma_b^D = \Gamma_b^{(0)} + \Gamma_b^{(1)} ,$$

with

$$\Gamma_b^{(1)} = -C_g f_\epsilon \frac{1}{\epsilon} \Gamma_b^{(0)} + C_b C_g (g_V^2 F_V + g_A^2 F_A) , \quad (2.13)$$

where the finite functions  $F_V$  and  $F_A$  are given in appendix B in terms of the form factors and  $\Gamma_b^{(0)}$  is given by eq. (2.3)

The  $O(\alpha_s)$  result, eq. (2.13), is divergent for  $\epsilon \rightarrow 0$  because the IR divergences associated with massless gluons running in the loops. To get a finite answer at this order we also need to include gluon bremsstrahlung from the quarks. This has to be computed by working in  $D$  dimensions.

The amplitude for the process  $Z \rightarrow b\bar{b}g$  (the two corresponding diagrams are given in fig. 1c) can be written as

$$\begin{aligned} T_{bg} = & \mu^{2\epsilon} \frac{g}{4c_W} g_s \bar{u}_1 \left( \frac{\gamma_\nu (\not{p}_1 + \not{k} + m_b) \gamma_\mu (g_V + g_A \gamma_5)}{2(p_1 k)} \right. \\ & \left. + \frac{\gamma_\mu (g_V + g_A \gamma_5) (-\not{p}_2 - \not{k} + m_b) \gamma_\nu}{2(p_2 k)} \right) \frac{\lambda^a}{2} v_2 \epsilon_a^\nu(k) \epsilon^\mu(q) . \end{aligned} \quad (2.14)$$

Here  $\lambda^a$  are the Gell-Mann  $SU(3)$  matrices, and  $\epsilon_a^\nu(k)$  is the gluon polarization vector.

The square of the amplitude, in dimension  $D$ , gives a rather involved expression that can be conveniently simplified when one realizes that the most divergent part of it factorizes completely, even in  $D$  dimensions, due to the factorization theorems for soft and collinear divergences.

Adding the three-body phase space (see appendix A) we find that the decay width of  $Z \rightarrow b\bar{b}g$  in  $D$  dimensions can be written as

$$\Gamma_{bg} = C_b C_g C_F \int dy_1 dy_2 \theta(h_p) h_p^{-\epsilon} A_{bg} , \quad (2.15)$$

where  $C_F = 4/3$  is the  $SU(3)$  group factor,  $y_1$  and  $y_2$  are defined in terms of the energy fractions of the two outgoing quarks

$$y_1 = 2(p_1 k)/m_Z^2 = 1 - 2E_2/m_Z , \quad y_2 = 2(p_2 k)/m_Z^2 = 1 - 2E_1/m_Z \quad (2.16)$$

and  $A_{bg}$  comes from the square of the matrix element,

$$A_{bg} = A_b \frac{h_p}{y_1^2 y_2^2} + g_V^2 h_V + g_A^2 h_A . \quad (2.17)$$

Here  $A_b$  is the same combination of couplings and masses that appears in the tree-level decay width to two quarks, eq. (2.5), and the function  $h_p$  is given by

$$h_p = y_1 y_2 (1 - y_1 - y_2) - r_b (y_1 + y_2)^2 , \quad (2.18)$$

and it is exactly the same function that defines the phase space available for the three-body decay (see eq. (2.15) and appendix A). After phase space integration this term will contain an IR divergence which comes from the singularity at  $y_1 = y_2 = 0$ .

The functions  $h_V$  and  $h_A$  describe the vector and the axial-vector parts of the remainder of the square of the amplitude which do not generate any IR divergence. In the limit  $\epsilon = 0$  they are given by:

$$h_V = \frac{1}{2} \left( \frac{y_2}{y_1} + \frac{y_1}{y_2} \right) , \quad (2.19)$$

$$h_A = (1 + 2r_b) h_V + 2r_b . \quad (2.20)$$

To perform the phase space integration it is convenient to change variables as follows

$$\begin{aligned} y_1 &= g(z) w , \\ y_2 &= g(z) z w , \end{aligned}$$

with

$$g(z) = \frac{z - r_b(1+z)^2}{z(1+z)} = \frac{1}{(1+c)^2} \frac{(z-c)(1-cz)}{z(1+z)} \quad (2.21)$$

and

$$c = \frac{1-\beta}{1+\beta} . \quad (2.22)$$

Then, both  $h_V$  and  $h_A$  only depend on the variable  $z$ , and the function  $h_p$ , which defines phase space and appears explicitly in eq. (2.17), factorizes completely

$$h_p = g(z)^3 z(1+z) w^2 (1-w) . \quad (2.23)$$

The function  $g(z)$  has zeros at  $z_1 = c$  and  $z_2 = 1/c$ . As phase space is defined by  $h_p > 0$  we obtain that the phase space in terms of the new variables is given by

$$c < z < 1/c \quad \text{and} \quad 0 < w < 1 . \quad (2.24)$$

After this change of variables eq. (2.15) can be rewritten as

$$\Gamma_{bg} = C_b C_g C_F \int_c^{1/c} dz g(z)^2 \int_0^1 dw w h_p^{-\epsilon} A_{bg} . \quad (2.25)$$

Now the  $w$  integration is very simple and leads to Beta functions. For the integration of the term of the amplitude proportional to  $A_b$  (see eq. (2.17)) we get

$$\int_c^{1/c} dz \int_0^1 dw h_p^{1-\epsilon} \frac{1}{g(z)^2 z^2 w^3} = B(-2\epsilon, 2-\epsilon) \int_c^{1/c} dz \frac{1}{g(z)^2 z^2} \left( g(z)^3 z(1+z) \right)^{1-\epsilon} , \quad (2.26)$$

where the function  $B(-2\epsilon, 2 - \epsilon)$  has a single pole in  $\epsilon = 0$ . In this way, all the divergent behaviour has been factorized in the Beta function. Then, to perform the  $z$  integration we can expand the integrant for small  $\epsilon$  and keep only terms linear in  $\epsilon$ . The integrations can be easily performed and the results written in terms of logarithms and dilogarithmic functions. The rest of the integrals do not lead to any divergence and can be done, without problem, putting  $\epsilon$  equal to zero.

After phase space integration, the decay width for  $Z \rightarrow b\bar{b}g$  can be written in the following form

$$\Gamma_{bg} = C_g f_\epsilon \frac{1}{\epsilon} \Gamma_b^{(0)} + C_b C_g \left( g_V^2 G_V + g_A^2 G_A \right), \quad (2.27)$$

where the first term contains the IR divergent part and the IR finite functions  $G_V$  and  $G_A$  are given in appendix B.

The IR divergent part of eq. (2.27) is identical, but with reversed sign, to the one obtained for  $\Gamma_b^{(1)}$ , therefore in the sum they will cancel, as it should be:

$$\Gamma_b = \Gamma_b^{(0)} + \Gamma_b^{(1)} + \Gamma_{bg} = \Gamma_b^{(0)} + C_b C_g \left( g_V^2 T_V + g_A^2 T_A \right), \quad (2.28)$$

with

$$T_V = F_V + G_V, \quad (2.29)$$

$$T_A = F_A + G_A. \quad (2.30)$$

From the results of the appendix B we can easily obtain the limit of these functions for small quark masses,  $m_b \ll m_Z$  ( $r_b \ll 1$ )

$$T_V \approx 1 + 12r_b, \quad (2.31)$$

$$T_A \approx 1 - 6r_b(2 \log r_b + 1). \quad (2.32)$$

If we plug this result into eq. (2.28) we obtain the well-known result [11]

$$\Gamma_b = m_Z \frac{g^2}{c_W^2 64\pi} \left[ g_V^2 \left( 1 + \frac{\alpha_s}{\pi} (1 + 12r_b) \right) + g_A^2 \left( 1 - 6r_b + \frac{\alpha_s}{\pi} (1 - 6r_b(2 \log r_b + 1)) \right) \right]. \quad (2.33)$$

It is interesting to note the presence of the large logarithm,  $\log(m_b^2/m_Z^2)$ , proportional to the quark mass in the axial part of the QCD corrected width, eq. (2.33). The mass that appears in all above calculations should be interpreted as the perturbative *pole* mass of the quark. But in principle the expression (2.33) could also be written in terms of the so-called *running* quark mass at the  $m_Z$  scale by using

$$m_b^2 = \bar{m}_b^2(m_Z) \left[ 1 + 2 \frac{\alpha_s}{\pi} \left( \log \left( \frac{m_Z^2}{m_b^2} \right) + \frac{4}{3} \right) \right]. \quad (2.34)$$

Then, we see that all large logarithms are absorbed in the running of the quark mass from the  $m_b$  scale to the  $m_Z$  scale [11] and we have

$$\Gamma_b = m_Z \frac{g^2}{c_W^2 64\pi} \left[ g_V^2 \left( 1 + \frac{\alpha_s}{\pi} (1 + 12\bar{r}_b) \right) + g_A^2 \left( 1 - 6\bar{r}_b + \frac{\alpha_s}{\pi} (1 - 22\bar{r}_b) \right) \right], \quad (2.35)$$

where  $\bar{r}_b = \bar{m}_b^2(m_Z)/m_Z^2$ .

This result means that the bulk of the QCD corrections depending on the mass could be accounted for by using tree-level expressions for the decay width but interpreting the quark

mass as the running mass at the  $m_Z$  scale. On the other hand, since  $\bar{m}_b(m_Z) \approx 3$  GeV is much smaller than the pole mass,  $m_b \approx 5$  GeV, it is clear that the quark mass corrections are much smaller than expected from the naïve use of the tree-level result with  $m_b \approx 5$  GeV, which would give mass corrections at the 1.8% level while in fact, once QCD corrections are taken into account, the mass corrections are only at the 0.7% level.

The final results of this section are well known but we find they could illuminate the discussion of mass effects in the two- and three-jet event rates and in the angular distribution with respect to the angle formed between the quark and gluon jets. Moreover the intermediate results of this section will be used in the rest of the paper.

### 3 Two- and three-jet event rates

According to our current understanding of the strong interactions, coloured partons, produced in hard processes, are hadronized and, at experiment, one only observes colourless particles. It is known empirically that, in high energy collision, final particles group in several clusters by forming energetic jets, which are related to the primordial partons. Thus, in order to compare theoretical predictions with experiments, it is necessary to define precisely what is a jet in both, parton level calculations and experimental measurements.

As we have seen in the previous section, at order  $\alpha_s$ , the decay widths of  $Z$  into both two and three partons are IR divergent. The two-parton decay rate is divergent due to the massless gluons running in the loops. The  $Z$ -boson decay width into three-partons has an IR divergence because massless gluons could be radiated with zero energy. The sum, however, is IR finite. Then it is clear that at the parton-level one can define an IR finite *two-jet decay rate*, by summing the two-parton decay rate and the IR divergent part of the three-parton decay width, e.g. integrated over the part of the phase space which contains soft gluon emission [19]. The integral over the rest of the phase space will give the *three-jet decay rate*. Thus we need to introduce a “resolution parameter” in the theoretical calculations in order to define IR-safe observables. Obviously, the resolution parameter, which defines the two- and the three-jet parts of the three-parton phase space should be related to the one used in the process of building jets from real particles.

In the last years the most popular definitions of jets are based on the so-called jet clustering algorithms. These algorithms can be applied at the parton level in the theoretical calculations and also to the bunch of real particles observed at experiment. It has been shown that, for some of the algorithms, the passage from partons to hadrons (hadronization) does not change much the behaviour of the observables [20], thus allowing to compare theoretical predictions with experimental results. In what follows we will use the word particles for both partons and real particles.

In the jet-clustering algorithms jets are defined as follows: starting from a bunch of particles with momenta  $p_i$  one computes, for example, a quantity like

$$y_{ij} = 2 \frac{E_i E_j}{s} (1 - \cos \theta_{ij})$$

for all pairs  $(i, j)$  of particles. Then one takes the minimum of all  $y_{ij}$  and if it satisfies that it is smaller than a given quantity  $y_c$  (the resolution parameter, y-cut) the two particles which define this  $y_{ij}$  are regarded as belonging to the same jet, therefore, they are recombined into a new pseudoparticle by defining the four-momentum of the pseudoparticle according to some rule, for example

$$p_k = p_i + p_j .$$



Algorithm	Resolution	Combination
EM	$2(p_i p_j)/s$	$p_k = p_i + p_j$
JADE	$2(E_i E_j)/s (1 - \cos \vartheta_{ij})$	$p_k = p_i + p_j$
E	$(p_i + p_j)^2/s$	$p_k = p_i + p_j$
DURHAM	$2 \min(E_i^2, E_j^2)/s (1 - \cos \vartheta_{ij})$	$p_k = p_i + p_j$

Table 1: The jet-clustering algorithms

After this first step one has a bunch of pseudoparticles and the algorithm can be applied again and again until all the pseudoparticles satisfy  $y_{ij} > y_c$ . The number of pseudoparticles found in the end is the number of jets in the event.

Of course, with such a jet definition the number of jets found in an event and its whole topology will depend on the value of  $y_c$ . For a given event, larger values of  $y_c$  will result in a smaller number of jets. In theoretical calculations one can define cross sections or decay widths into jets as a function of  $y_c$ , which are computed at the parton level, by following exactly the same algorithm. This procedure leads automatically to IR finite quantities because one excludes the regions of phase space that cause trouble. The success of the jet-clustering algorithms is due, mainly, to the fact that the cross sections obtained after the hadronization process agree quite well with the cross-sections calculated at the parton level when the same clustering algorithm is used in both theoretical predictions and experimental analyses.

There are different successful jet-clustering algorithms and we refer to refs. [20, 21] for a detailed discussion and comparison of these algorithms in the case of massless quarks.

In the rest of the paper we will use the four jet-clustering algorithms listed in the table 1, where  $\sqrt{s}$  is the total centre of mass energy. In addition to the well-known JADE, E and DURHAM algorithms we will use a slight modification of the JADE scheme particularly useful for analytical calculations with massive quarks. It is defined by the two following equations

$$y_{ij} = 2 \frac{p_i p_j}{s}$$

and

$$p_k = p_i + p_j$$

We will denote this algorithm as the EM scheme. For massless particles and at the lowest order E, JADE and EM give the same answers. However already at order  $\alpha_s^2$  they give different answers since after the first recombination the pseudoparticles are not massless anymore and the resolution functions are different.

For massive quarks the three algorithms, E, JADE and EM are already different at order  $\alpha_s$ . The DURHAM ( $K_T$ ) algorithm, which has been recently considered in order to avoid exponentiation problems present in the JADE algorithm [20, 22], is of course completely different from the other algorithms we use, both in the massive and the massless cases.

In figure 2 we plotted the phase-space for two values of  $y_c$  ( $y_c = 0.04$  and  $y_c = 0.14$ ) for all four schemes (the solid line defines the whole phase space for  $Z \rightarrow q\bar{q}g$  with  $m_q = 10$  GeV).

There is an ongoing discussion on which is the best algorithm for jet clustering in the case of massless quarks. The main criteria followed to choose them are based in two requirements:

1. Minimize higher order corrections.

2. Keep the equivalence between parton and hadronized cross sections.

To our knowledge no complete comparative study of the jet-clustering algorithms has been done for the case of massive quarks. The properties of the different algorithms with respect to the above criteria can be quite different in the case of massive quarks from those in the massless case. The first one because the leading terms containing double-logarithms of  $y$ -cut ( $\log^2(y_c)$ ) that appear in the massless calculation (at order  $\alpha_s$ ) and somehow determine the size of higher order corrections are substituted in the case of massive quarks by single-logarithms of  $y_c$  times a logarithm of the quark mass. The second one because hadronization corrections for massive quarks could be different from the ones for massless quarks.

Therefore, we will not stick to any particular algorithm but rather present results and compare them for all the four algorithms listed in the table 1.

### 3.1 The analytic calculation for the EM scheme

Here we calculate analytically, at leading order, the three-jet decay rate of the  $Z$ -boson by using the EM clustering algorithm.

At the parton level the two-jet region in the decay  $Z \rightarrow b\bar{b}g$  is given, in terms of the variables  $y_1$  and  $y_2$ , by the following conditions:

$$y_1 < y_c \quad \text{or} \quad y_2 < y_c \quad \text{or} \quad 1 - 2r_b - y_1 - y_2 < y_c. \quad (3.1)$$

This region contains the IR singularity,  $y_1 = y_2 = 0$  and the rate obtained by the integration of the amplitude over this part of the phase space should be added to the one-loop corrected decay width for  $Z \rightarrow b\bar{b}$ . The sum of these two quantities is of course IR finite and it is the so-called two-jet decay width at order  $\alpha_s$ . The integration over the rest of the phase space defines the three-jet decay width at the leading order. It is obvious that the sum of the two-jet and three-jet decay widths is independent of the resolution parameter  $y_c$ , IR finite and given by the quantity  $\Gamma_b = \Gamma(Z \rightarrow b\bar{b} + b\bar{b}g + \dots)$  calculated in section 2. Therefore we have

$$\Gamma_b = \Gamma_{2j}^b(y_c) + \Gamma_{3j}^b(y_c) + \dots$$

Clearly, at order  $\alpha_s$ , knowing  $\Gamma_b$  and  $\Gamma_{3j}^b(y_c)$  we can obtain  $\Gamma_{2j}^b(y_c)$  as well.

The calculation of  $\Gamma_{3j}^b(y_c)$  at order  $\alpha_s$  is a tree-level calculation and does not have any IR problem since the soft gluon region has been excluded from phase space. Therefore the calculation can be done in four dimensions without trouble.

We will start with equation (2.15) taking  $\epsilon = 0$  and with the phase space constrained by the cuts defined in eq. (3.1).

$$\Gamma_{3j}^b = \left( C_b C_g C_F \int dy_1 dy_2 \theta_{PS} \theta_c A_{bg} \right)_{\epsilon=0}, \quad (3.2)$$

where the  $\theta$  function

$$\theta_{PS} = \theta(h_p) \quad (3.3)$$

gives the whole phase space, and the product of  $\theta$  functions

$$\theta_c = \theta(y_2 - y_c) \theta(y_1 - y_c) \theta(1 - 2r_b - y_1 - y_2 - y_c) \quad (3.4)$$

introduces the appropriate cuts for the EM scheme. The square of the amplitude,  $A_{bg}$ , is given in eq. (2.17). The phase space and the cuts are represented in the first plot of fig. 2.

Depending on the value of  $y_c$  the limits of integration are different, there are three cases which correspond to three different topologies of the overlapping of the phase space and the area defined by the cuts:

$$\begin{aligned} y_c &< 2r_b \\ 2r_b &< y_c < \bar{y}_c \\ \bar{y}_c &< y_c \end{aligned} , \quad (3.5)$$

where  $\bar{y}_c = \sqrt{r_b}(1 - \sqrt{r_b}) + O(r_b^2\sqrt{r_b})$  is given by a solution of the following equation

$$4(1 - 2y_c - 2r_b)^2(y_c^2 + 4r_b) = y_c^2(2 - y_c - 8r_b)^2. \quad (3.6)$$

Since the integrant is symmetric under the exchange  $y_1 \leftrightarrow y_2$  we can restrict the region of integration to the region  $y_1 > y_2$  (multiplying the result by a factor 2). In addition it is useful to change variables as before,  $y_2 = zy_1$ . We will not discuss the technical details of the calculation here; all of the integrals can be reduced to logarithmic and dilogarithmic functions and the final result can be written in the following form

$$\Gamma_{3j}^b = C_b C_g \left( g_V^2 H_V^{(0)}(y_c, r_b) + g_A^2 H_A^{(0)}(y_c, r_b) \right), \quad (3.7)$$

where the superscript  $(0)$  in the functions  $H_{V(A)}^{(0)}(y_c, r_b)$  reminds us that this is only the lowest order result. Analytical expressions for the functions  $H_V^{(0)}(y_c, r_b)$  and  $H_A^{(0)}(y_c, r_b)$  are given in appendix C. Obviously, the general form (3.7) is independent of what particular jet-clustering algorithm has been used.

In the limit of zero masses,  $r_b = 0$ , chirality is conserved and the two functions  $H_V^{(0)}(y_c, r_b)$  and  $H_A^{(0)}(y_c, r_b)$  become identical

$$H_V^{(0)}(y_c, 0) = H_A^{(0)}(y_c, 0) \equiv A^{(0)}(y_c).$$

In this case we obtain the known result for the JADE-type algorithms, which is expressed in terms of the function  $A^{(0)}(y_c)$  also given in appendix C<sup>3</sup>.

To see more clearly the size of mass effects we are going to study the following ratio of jet fractions

$$R_3^{bd} \equiv \frac{\Gamma_{3j}^b(y_c)/\Gamma^b}{\Gamma_{3j}^d(y_c)/\Gamma^d} = \left( c_V \frac{H_V^{(0)}(y_c, r_b)}{A^{(0)}(y_c)} + c_A \frac{H_A^{(0)}(y_c, r_b)}{A^{(0)}(y_c)} \right) (1 + 6r_b c_A + O(r_b^2)), \quad (3.8)$$

where we have defined

$$c_V = \frac{g_V^2}{g_V^2 + g_A^2}, \quad c_A = \frac{g_A^2}{g_V^2 + g_A^2}.$$

In eq. (3.8) we have kept only the lowest order terms in  $\alpha_s$  and  $r_b$ . The last factor is due to the normalization to total rates. This normalization is important from the experimental point of view but also from the theoretical point of view because in these quantities large weak corrections dependent on the top quark mass [23] cancel. Note that, for massless quarks, the ratio  $\Gamma_{3j}^d(y_c)/\Gamma^d$  is independent on the neutral current couplings of the quarks and, therefore, it is the same for up- and down-quarks and given by the function  $A^{(0)}$ . This means that we could equally use the normalization to any other light quark or to the sum of all of them (including also the c-quark if its mass can be neglected).

---

<sup>3</sup>Note that with our normalization  $A^{(0)}(y_c) = \frac{1}{2}A(y_c)$ , with  $A(y_c)$  defined in ref. [20].

### 3.2 Estimate of higher order contributions

All previous results come from a tree-level calculation, however, as commented in the introduction, we do not know what is the value of the mass we should use in the final results since the difference among the pole mass, the running mass at  $\mu = m_b$  or the running mass at  $\mu = m_Z$  are next-order effects in  $\alpha_s$ .

In the case of the inclusive decay rate we have shown that one could account (with very good precision) for higher order corrections by using the running mass at the  $m_Z$  scale in the lowest order calculations. Numerically the effect of running the quark mass from  $m_b$  to  $m_Z$  is very important.

One could also follow a similar approach in the case of jet rates and try to account for the next-order corrections by using the running quark mass at different scales. We will see below that the dependence of  $R_3^{bd}$  on the quark mass is quite strong (for all clustering schemes); using the different masses (e.g.  $m_b$  or  $\bar{m}_b(M_Z)$ ) could amount to almost a factor 2 in the mass effect. This suggests that higher order corrections could be important. Here, however, the situation is quite different, since in the decay rates to jets we have an additional scale given by  $y_c$ ,  $E_c \equiv m_Z \sqrt{y_c}$ , e.g. for  $y_c = 0.01$  we have  $E_c = 9$  GeV and for  $y_c = 0.05$ ,  $E_c = 20$  GeV. Perhaps one can absorb large logarithms,  $\log(m_b/m_Z)$  by using the running coupling and the running mass at the  $\mu = m_Z$  scale, but there will remain logarithms of the resolution parameter,  $\log(y_c)$ . For not very small  $y_c$  one can expect that the tree-level results obtained by using the running mass at the  $m_Z$  scale are a good approximation, however, as we already said, the situation cannot be settled completely until a next-to-leading calculation including mass effects is available.

Another way to estimate higher order effects in  $R_3^{bd}$  is to use the known results for the massless case [20, 21, 24]

Including higher order corrections the general form of eq. (3.7) is still valid with the change  $H_{V(A)}^{(0)}(y_c, r_b) \rightarrow H_{V(A)}(y_c, r_b)$ . Now we can expand the functions  $H_{V(A)}(y_c, r_b)$  in  $\alpha_s$  and factorize the leading dependence on the quark mass as follows

$$H_{V(A)}(y_c, r_b) = A^{(0)}(y_c) + \frac{\alpha_s}{\pi} A^{(1)}(y_c) + r_b \left( B_{V(A)}^{(0)}(y_c, r_b) + \frac{\alpha_s}{\pi} B_{V(A)}^{(1)}(y_c, r_b) \right) + \dots \quad (3.9)$$

In this equation we already took into account that for massless quarks vector and axial contributions are identical<sup>4</sup>

Then, we can rewrite the ratio  $R_3^{bd}$ , at order  $\alpha_s$ , as follows

$$\begin{aligned} R_3^{bd} = 1 + r_b & \left[ c_V \frac{B_V^{(0)}(y_c, r_b)}{A^{(0)}(y_c)} \left( 1 + \frac{\alpha_s}{\pi} \left( \frac{B_V^{(1)}(y_c, r_b)}{B_V^{(0)}(y_c, r_b)} - \frac{A^{(1)}(y_c)}{A^{(0)}(y_c)} \right) \right) \right. \\ & \left. + c_A \frac{B_A^{(0)}(y_c, r_b)}{A^{(0)}(y_c)} \left( 1 + \frac{\alpha_s}{\pi} \left( \frac{B_A^{(1)}(y_c, r_b)}{B_A^{(0)}(y_c, r_b)} - \frac{A^{(1)}(y_c)}{A^{(0)}(y_c)} \right) \right) \right] \\ & \times \left( 1 + 6r_b \left( c_A \left( 1 + 2 \frac{\alpha_s}{\pi} \log(r_b) \right) - c_V 2 \frac{\alpha_s}{\pi} \right) \right) . \end{aligned} \quad (3.10)$$

From the calculations in this paper we know  $B_V^{(0)}(y_c, r_b)$  and  $B_A^{(0)}(y_c, r_b)$ ; the lowest order function for the massless case,  $A^{(0)}(y_c)$ , is also known analytically for JADE-type algorithms,

---

<sup>4</sup>This is not completely true at  $O(\alpha_s^2)$  because the triangle anomaly: there are one-loop triangle diagrams contributing to  $Z \rightarrow b\bar{b}g$  with the top and the bottom quarks running in the loop. Since  $m_t \neq m_b$  the anomaly cancellation is not complete. These diagrams contribute to the axial part even for  $m_b = 0$  and lead to a deviation from  $A_V^{(1)}(y_c) = A_A^{(1)}(y_c)$  [25]. This deviation is, however, small [25] and we are not going to consider its effect here.

eq. (C.13) and refs. [20, 21], and for the DURHAM algorithm [22]. A parameterization of the function  $A^{(1)}(y_c)$  can be found in [20] for the different algorithms<sup>5</sup>. As we already mentioned this function is different for different clustering algorithms. The only unknown functions in eq. (3.10) are  $B_V^{(1)}(y_c, r_b)$  and  $B_A^{(1)}(y_c, r_b)$ , which must be obtained from a complete calculation at order  $\alpha_s^2$  including mass effects (at least at leading order in  $r_b$ ).

Nevertheless, in order to estimate the impact of higher order corrections in our calculation we will assume that  $B_{V,A}^{(1)}(y_c, r_b)/B_{V,A}^{(0)}(y_c, r_b) \ll A^{(1)}(y_c)/A^{(0)}(y_c)$  and take  $A^{(1)}(y_c)/A^{(0)}(y_c)$  from<sup>6</sup> [20, 21]. Of course this does not need to be the case but at least it gives an idea of the size of higher order corrections. We will illustrate the numerical effect of these corrections for  $R_3^{bd}$  in the next subsection. As we will see, the estimated effect of next-order corrections is quite large, therefore in order to obtain the  $b$ -quark mass from these ratios the calculation of the functions  $B_{V,A}^{(1)}(y_c, r_b)$  is mandatory [26].

### 3.3 Numerical results for $R_3^{bd}$ for different clustering algorithms

To complete this section we present the numerical results for  $R_3^{bd}$  calculated with the different jet-clustering algorithms. For the JADE, E and Durham algorithms we obtained the three-jet rate by a numerical integration over the phase-space given by the cuts (see fig. 2). For the EM scheme we used our analytical results which were also employed to cross check the numerical procedure.

In fig. 3 we present the ratio  $R_3^{bd}$ , obtained by using the tree-level expression, eq. (3.8), against  $y_c$  for  $m_b = 5$  GeV and  $m_b = 3$  GeV. We also plot the results given by eq. (3.10) (with  $B_{V,A}^{(1)}(y_c, r_b)/B_{V,A}^{(0)}(y_c, r_b) = 0$ ) for  $m_b = 5$  GeV, which gives an estimate of higher order corrections. For  $y_c < 0.01$  we do not expect the perturbative calculation to be valid.

As we see from the figure, the behaviour of  $R_3^{bd}$  is quite different in the different schemes. The mass effect has a negative sign for all schemes except for the E-algorithm. For  $y_c > 0.05$  the mass effects are at the 4% level for  $m_b = 5$  GeV and at the 2% level for  $m_b = 3$  GeV (when the tree level expression is used). Our estimate of higher order effects, with the inclusion of the next-order effects in  $\alpha_s$  for massless quarks, shifts the curve for  $m_b = 5$  GeV in the direction of the 3 GeV result and amounts to about of 20% to 40% of the difference between the tree-level calculations with the two different masses. For both E and EM schemes we used the higher order results for the E scheme.

For the JADE algorithm we have also plotted in fig. 3 the experimental results for  $R_3^{bd}$  obtained by the DELPHI group [2] on the basis of the data collected in 1990-1991. The experimental errors, due to the limited statistics analyzed, are rather large. However, one can already see the effect of the quark mass. If the  $b$ -quark mass would be zero, one should obtain a ratio  $R_3^{bd}$  constant and equal to 1. It is clearly seen from the figure that for  $y_c < 0.08$  the data are significantly below 1. For larger values of  $y_c$ , the number of events decreases, the errors become too large and the data are consistent with 1. When larger amount of data is analyzed and the experimental error is decreased, it will be very interesting to see if data will exhibit the different signs of the mass effect in  $R_3^{bd}$  (positive for the E scheme and negative for the other schemes) as predicted by our parton level calculations (see fig. 3).

In spite of the fact that the effect of the quark mass in  $R_3^{bd}$  has been seen, it is too early, in our opinion, to extract now the value of the  $b$ -quark mass from the data. As discussed above the higher order corrections to  $R_3^{bd}$  are presumably rather large and should be included in the

<sup>5</sup>With our choice of the normalization  $A^{(1)}(y_c) = B(y_c)/4$ , where  $B(y_c)$  is defined in [20].

<sup>6</sup>For the EM algorithm this function has not yet been computed. To make an estimate of higher order corrections we will use in this case the results for the E algorithm.

Algorithm	$k_V^{(0)}$	$k_V^{(1)}$	$k_V^{(2)}$	$k_A^{(0)}$	$k_A^{(1)}$	$k_A^{(2)}$
EM	-2.72	-14.64	-28.58	-2.61	-13.54	-30.67
JADE	-2.01	- 5.19	-13.25	-1.90	-4.13	-15.42
E	4.68	19.04	25.97	4.71	19.81	23.39
DURHAM	-1.69	- 4.76	-12.70	-1.65	-4.28	-15.48

Table 2: Results of the tree parameter fits of the functions  $B_{V,A}^{(0)}(y_c, r_b)/A^{(0)}(y_c) = \sum_{n=0}^2 k_{V,A}^{(n)} \log^n y_c$  in the range  $0.01 < y_c < 0.2$

theoretical calculations. However, it is clear, that once the essential next-to-leading order corrections will be available and all LEP data will be included in the analysis, the ratios  $R_3^{bd}$  will certainly allow for a reasonable determination of the  $b$ -quark mass and for a check of its running from  $m_b$  to  $m_Z$ .

To simplify the use of our results we present simple fits to the ratios  $B_{V,A}^{(0)}(y_c, r_b)/A^{(0)}(y_c)$ , which define  $R_3^{bd}$  at lowest order, for the different clustering algorithms. We use the following parameterization:

$$B_{V,A}^{(0)}(y_c, r_b)/A^{(0)}(y_c) = \sum_{n=0}^2 k_{V,A}^{(n)} \log^n y_c, \quad (3.11)$$

and the results of the fits for the range  $0.01 < y_c < 0.2$  are presented in table 2.

In fig. 4 we plot the ratios  $B_{V,A}^{(0)}(y_c, r_b)/A^{(0)}(y_c)$  as a function of  $y_c$  for the different algorithms (dashed lines for  $m_b = 5$  GeV, dotted lines for  $m_b = 3$  GeV and solid curves for the result of our fits). As we see from the figure the remnant mass dependence in these ratios (in the range of masses we are interested in and in the range of  $y_c$  we have considered) is rather small and for actual fits we used the average of the ratios for the two different masses. We see from these figures that such a simple three-parameter fit works reasonably well for all the algorithms.

Concluding this section we would like to make the following remark. In this paper we discuss the  $Z$ -boson decay. In LEP experiments one studies the process  $e^+e^- \rightarrow (Z\gamma^*) \rightarrow b\bar{b}$  and, apart from the resonant  $Z$ -exchange cross section, there are contributions from the pure  $\gamma$ -exchange and from the  $\gamma - Z$ -interference. The non-resonant  $\gamma$ -exchange contribution at the peak is less than 1% for muon production and in the case of  $b$ -quark production there is an additional suppression factor  $Q_b^2 = 1/9$ . In the vicinity of the  $Z$ -peak the interference is also suppressed because it is proportional to  $Q_b(s - m_Z^2)$  ( $\sqrt{s}$  is the  $e^+e^-$  centre of mass energy). We will neglect these terms as they give negligible contributions compared with the uncertainties in higher order QCD corrections to the quantities we are considering.

Obviously, QED initial-state radiation should be taken into account in the real analysis; the cross section for  $b$ -pair production at the  $Z$  resonance can be written as

$$\sigma_{b\bar{b}}(s) = \int \sigma_{b\bar{b}}^0(s') F(s'/s) ds' \quad (3.12)$$

where  $F(s'/s)$  is the well-known QED radiator for the total cross section [27] and, the Born cross section, neglecting pure  $\gamma$  exchange contribution and the  $\gamma - Z$ -interference, has the form

$$\sigma_{b\bar{b}}^0(s) = \frac{12\pi\Gamma_e\Gamma_b}{m_Z^2} \frac{s}{(s - m_Z^2)^2 + m_Z^2\Gamma_Z^2} \quad (3.13)$$

with obvious notation. Note that  $\Gamma_b$  in this expression can be an inclusive width as well as some more exclusive quantity, which takes into account some kinematical restrictions on the final state.

## 4 Angular distribution

If the gluon jet can be identified with enough efficiency, an interesting quantity which is very sensitive to the IR behaviour of the amplitudes is the angular distribution with respect to the angle formed between one of the quark jets and the gluon jet<sup>7</sup>. If  $\vartheta_1$  ( $\vartheta_2$ ) is the angle between the quark (antiquark) and the gluon jets we define  $\vartheta = \min(\vartheta_1, \vartheta_2)$ . We want to obtain the angular distribution with respect to  $\vartheta$ . The starting point is eq. (3.2) where we change variables from one of the  $y_1$  or the  $y_2$  variables to  $\vartheta$ . To do this we take into account that the amplitude is completely symmetric in  $y_1$  and  $y_2$ , therefore we can restrict the integration only to the region  $y_2 > y_1$  and add a factor 2. In that region  $\vartheta = \vartheta_1$ . Therefore to obtain the distribution with respect to  $\vartheta$  it is enough to obtain the distribution with respect to  $\vartheta_1$  but constraining the phase space integration to  $y_2 > y_1$ .

For  $y_2 > y_1$  we can easily express  $y_1$  in terms of  $\cos \vartheta = \cos \vartheta_1$  as follows

$$y_1 = \frac{y_2 \left(1 - y_2 - \cos \vartheta \sqrt{(1 - y_2)^2 - 4r_b}\right)}{1 + y_2 + \cos \vartheta \sqrt{(1 - y_2)^2 - 4r_b}}. \quad (4.1)$$

Adding the Jacobian of the transformation we find from eq. (3.2) (taking  $\epsilon = 0$  as this quantity is IR convergent)

$$\frac{d\Gamma_{3j}^b}{d\vartheta} = C_b C_g C_F 2 \int dy_2 \theta_{PS} \theta_c \theta(y_2 - y_1) \sin \vartheta \frac{2y_2 \sqrt{(1 - y_2)^2 - 4r_b}}{\left(1 + y_2 + \cos \vartheta \sqrt{(1 - y_2)^2 - 4r_b}\right)^2} A_{bg}, \quad (4.2)$$

where  $y_1$  is expressed in terms of  $\cos \vartheta$  and  $y_2$  using eq. (4.1).

In order to see how large mass effects are in this angular distribution we define the following ratio of angular distributions:

$$R_{\vartheta}^{bd} = \frac{1}{\Gamma^b} \frac{d\Gamma_{3j}^b}{d\vartheta} \bigg/ \frac{1}{\Gamma^d} \frac{d\Gamma_{3j}^d}{d\vartheta} \quad (4.3)$$

In the case of massless quarks the integration limits in eq. (4.2) can be found analytically for the JADE-type schemes and the result of the integration over  $y_2$  is expressed in terms of logarithms involving  $\vartheta$  and  $y_c$ . We find

$$\frac{1}{\Gamma^d} \frac{d\Gamma_{3j}^d}{d\vartheta} = \frac{\alpha_s}{\pi} f_{\vartheta}(y_c), \quad (4.4)$$

where the function  $f_{\vartheta}(y_c)$  is given analytically in appendix D for the JADE-type schemes and represented in fig. 5 for the JADE-type and the Durham algorithms for different values of  $y_c$  ( $y_c = 0.02$  (solid line),  $y_c = 0.04$  (dashed line),  $y_c = 0.06$  (dotted line) and  $y_c = 0.08$  (dash-dotted line)). We observe a very sharp peak, for both algorithms, in the region of  $90^\circ$ – $100^\circ$  depending on the value of  $y_c$ , for  $y_c = 0.04$  the peak is at about  $92^\circ$  for the JADE-type algorithms and at about  $99^\circ$  for the Durham algorithm. We see that the absolute size of the peak is a factor two larger in the case of the JADE-type algorithms (for the same value of  $y_c$ )

---

<sup>7</sup>We thank J. Fuster for suggesting us the study of this observable.

than in the case of the DURHAM scheme. This is due to the difference of phase spaces for two schemes.

For massive quarks, although the integrations can still be performed analytically in the EM scheme, some of the integration limits are solutions of polynomial equations of the third degree and the analytical result is not especially enlightening. Then, we have computed the ratio  $R_{\vartheta}^{bd}$  by doing the one-dimensional integration in (4.2) numerically.

Numerical results for  $R_{\vartheta}^{bd}$  are presented in fig. 6 for the different algorithms for  $y_c = 0.04$  and for both  $m_b = 5$  GeV (solid line) and for  $m_b = 3$  GeV (dashed line). In all cases we plot the ratios for the interval of angles for which the differential cross section is still sizable (see fig. 5), i.e.  $\vartheta \approx 45^\circ - 120^\circ$  for JADE-type schemes and  $\vartheta \approx 50^\circ - 130^\circ$  for the DURHAM algorithm. For small angles and  $m_b = 5$  GeV the effect can be as large as 10% of the ratio. Note, however, that the angular distribution, fig. 5, drops down rapidly for such small angles. In addition, since the ratio changes very fast in this region the exact size of the effect will depend on the angular resolution achieved at experiment.

As in the case of ratios of three-jet event rates,  $R_3^{bd}$ , the variation of the ratio of angular distributions,  $R_{\vartheta}^{bd}$ , for  $m_b = 5$  GeV and  $m_b = 3$  GeV gives a measure of the size of higher order corrections.

We observe in all the ratios the irregular behaviour in the region where the massless angular distribution peaks. This is due to the fact that in the massive case the position of the peak is slightly shifted with respect to the massless case. The mismatch between the two peaks appears as a discontinuity in the ratio when seen from large scales.

It will be interesting to see if data really follow these patterns for  $R_{\vartheta}^{bd}$ . A preliminary analysis performed by the DELPHI group [28] seems to indicate that, indeed, data do follow these angular distributions, at least qualitatively, and exhibit the variations present in the different algorithms.

## 5 Discussion and conclusions

In this paper we have presented a theoretical study of quark-mass effects in the decay of the  $Z$ -boson into bottom quarks.

First, we have reproduced, with the complete mass dependences, the results for the inclusive decay rate of the  $Z \rightarrow b\bar{b} + \dots$  to order  $\alpha_s$  by adding gluon bremsstrahlung from the  $b$ -quarks to the one-loop corrected decay width of  $Z \rightarrow b\bar{b}$ . Although the sum of the two contributions is finite, each of them is separately IR divergent. We used dimensional continuation to regularize the IR divergences and gave a complete analytical result in arbitrary space-time dimensions for each of the two contributions.

The main contribution of this paper is, however, the analysis of some three-jet observables which are more sensitive to the value of the quark masses.

For a slight modification of the JADE algorithm (the EM algorithm) we have calculated analytically the three-jet decay width of the  $Z$ -boson into  $b$ -quarks as a function of the jet resolution parameter,  $y_c$ , and the  $b$ -quark mass. The answer is rather involved, but can be expressed in terms of elementary functions. Apart from the fact that these analytical calculations are interesting by themselves, they can also be used to test Monte Carlo simulations. For the EM, JADE, E and DURHAM clustering algorithms we have obtained the three-jet decay width by a simple two-dimensional numerical integration. Numerical and analytical results have been compared in the case of the EM scheme.



We discussed quark-mass effects by considering the quantity

$$R_3^{bd} = \frac{\Gamma_{3j}^b(y_c)/\Gamma^b}{\Gamma_{3j}^d(y_c)/\Gamma^d} = 1 + \frac{m_b^2}{m_Z^2} F(m_b, y_c)$$

which has many advantages from both the theoretical and the experimental point of views. In particular, at lowest order, the function  $F(m_b, y_c)$  is almost independent on the quark mass (for the small values of the mass in which we are interested in) and has absolute values ranging from 10 to 35 (depending on  $y_c$  and on the algorithm), where the larger values are obtained for  $y_c$  of about 0.01.

At the lowest order in  $\alpha_s$  we do not know what is the exact value of the quark mass that should be used in the above equation since the difference between the different definitions of the  $b$ -quark mass, the pole mass,  $m_b \approx 5$  GeV, or the running mass at the  $m_Z$ -scale,  $\bar{m}_b(m_Z) \approx 3$  GeV, is order  $\alpha_s$ . Therefore, we have presented all results for these two values of the mass and have interpreted the difference as an estimate of higher order corrections. Conversely one can keep the mass fixed and include in  $F(m_b, y_c)$  higher order corrections already known for the massless case. According to these estimates the  $O(\alpha_s)$  corrections can be about 40% of the tree-level mass effect (depending on the clustering scheme), although we cannot exclude even larger corrections.

By using the lowest order result we find that for moderate values of the resolution parameter,  $y_c \approx 0.05$ , the mass effect in the ratio  $R_3^{bd}$  is about 4% if the pole mass value of the  $b$ -quark,  $m_b \approx 5$  GeV, is used, and the effect decreases to 2% if  $m_b = 3$  GeV.

We have compared our predictions for  $R_3^{bd}$  for the JADE algorithm, with the results obtained from the 1990-1991 data by the DELPHI group [2]. Although the errors obtained in the analysis of this limited sample of data are rather large, especially for  $y_c > 0.08$ , one clearly sees that for small values of  $y$ -cut ( $y_c < 0.08$ ) the experimental points are systematically below 1, thus clearly exhibiting the effect of the mass of the quark, as for massless quark  $R_3^{bd} = 1$ . The size of the effect agrees roughly with the predictions. One can expect the reduction of the experimental error by, at least, a factor two when the data collected in 1992 are included in the analysis. Then, mass effects will be more clearly seen and it will be very interesting to see if data follow the different qualitative behaviour of the ratio  $R_3^{bd}$  as a function of  $y_c$  as predicted by the parton model calculations (positive effect for the E scheme and negative mass effect for the other algorithms). However, in order to extract a meaningful value of the  $b$ -quark mass from the data it will be necessary to include next-to-leading order corrections since the leading mass effect we have calculated does not distinguish among the different definitions of the quark mass (pole mass, running mass at the  $m_b$  scale or running mass at the  $m_Z$  scale). We believe that the future analysis of the whole LEP statistics and its comparison with the theoretical predictions for the three-jet ratios, which meet the future experimental precision, will allow for a good determination of the  $b$ -quark mass at the highest energy scale and for a check of its running from  $m_b$  to  $m_Z$ .

The high precision achieved at LEP allows for a good separation of the gluonic and quark jets and a measurement of the angular distribution of the radiated gluon with respect to the quark momenta. This angular distribution has been calculated for massless quarks analytically for the JADE-type schemes and numerically for the DURHAM algorithm. We have studied the mass effects, for the different jet-clustering algorithms, in the quantity

$$R_\theta^{bd} = \frac{1}{\Gamma^b} \frac{d\Gamma_{3j}^b}{d\theta} \bigg/ \frac{1}{\Gamma^d} \frac{d\Gamma_{3j}^d}{d\theta}.$$

We have shown that, for a reasonable value of the resolution parameter,  $y_c = 0.04$ , the mass effects in this ratio can be as large as 10% of the ratio for  $m_b = 5$  GeV (depending on the

algorithm, the angle  $\vartheta$  and the angular resolution). The larger values are obtained for small angles where, however, the angular distribution falls down very rapidly. A fit to this ratio can be used to extract the value of the  $b$ -quark mass. It will be interesting to see if data really follow the predictions for the angular distributions and if the mass effects in the ratio of angular distributions are well described by our results.

Concluding, we have raised the question of the possibility of measuring the  $b$ -quark mass at LEP by using three-jet observables. In our opinion, this is a big challenge for both experimentalists and theorists. Clearly, more work has to be done in order the precision of theoretical predictions meet the experimental accuracy, in particular order  $\alpha_s^2$  calculations and studies of hadronization corrections including mass effects will be needed. However, this effort is worth since it will allow for an independent measurement of  $m_b$  at much larger energies where, presumably, non-perturbative effects are negligible.

## Acknowledgements

We would like to thank J. Fuster for his continuous encouragement, for many helpful discussions and for carefully reading the manuscript. G. Rodrigo acknowledges the CERN theory group for its hospitality during the preparation of this work and the Conselleria de Cultura, Educació i Ciència de la Generalitat Valenciana for financial support. This work was supported in part by CICYT, Spain, under grant AEN93-0234.

# APPENDICES

## A Phase space in $D = 4 - \epsilon$ dimensions

The phase space for  $n$ -particles in the final state in  $D$ -dimensions [18] ( $D = 4 - 2\epsilon$ ) has the following general form

$$d(P S_n) = (2\pi)^D \prod_{i=1,n} \frac{d^{D-1} p_i}{(2\pi)^{D-1} 2E_i} \delta^D \left( q - \sum_{i=1,n} p_i \right) \quad (\text{A.1})$$

$$= (2\pi)^D \prod_{i=1,n} \frac{d^D p_i}{(2\pi)^{D-1} 2E_i} \delta(p_i^2 - m_i^2) \Theta(E_i) \delta^D \left( q - \sum_{i=1,n} p_i \right). \quad (\text{A.2})$$

Then doing several trivial integrations we have the following phase-space factor for the process  $Z \rightarrow b\bar{b}$

$$P S_2 = \frac{1}{4\pi} \frac{\beta}{2} \frac{\Gamma(1-\epsilon)}{\Gamma(2-2\epsilon)} \left( \frac{\beta^2 m_Z^2}{4\pi} \right)^{-\epsilon}, \quad (\text{A.3})$$

where  $\beta = \sqrt{1 - 4r_b}$  with  $r_b = m_b^2/m_Z^2$ ,

For the case of the decay into three particles,  $Z \rightarrow b\bar{b}g$ , we have

$$d(P S_3) = \frac{m_Z^2}{16(2\pi)^3} \frac{1}{\Gamma(2-2\epsilon)} \left( \frac{m_Z^2}{4\pi} \right)^{-2\epsilon} \theta(h_p) h_p^{-\epsilon} dy_1 dy_2, \quad (\text{A.4})$$

where the function  $h_p$  which gives a phase-space boundary in terms of variables  $y_1 = 2(p_1 k)/m_Z^2$  and  $y_2 = 2(p_2 k)/m_Z^2$  has the form

$$h_p = y_1 y_2 (1 - y_1 - y_2) - r_b (y_1 + y_2)^2. \quad (\text{A.5})$$

## B Inclusive decay rate functions

In this section we collect the functions needed in section 2. The relevant form factors are:

$$f_\epsilon = C_F \left( 1 + \frac{1 + \beta^2}{2\beta} \log(c) \right), \quad (\text{B.1})$$

$$f_{Tf} = C_F \frac{1 - \beta^2}{2\beta} \log(c), \quad (\text{B.2})$$

$$\begin{aligned} f_{Af} &= f_\epsilon \log(r_b) + C_F \left[ -2 - \frac{2 + \beta^2}{2\beta} \log(c) \right. \\ &\quad \left. + \frac{1 + \beta^2}{\beta} \left( \text{Li}_2(c) + \frac{\pi^2}{3} - \frac{1}{4} \log^2(c) + \log(c) \log(1 - c) \right) \right]. \end{aligned} \quad (\text{B.3})$$

In the expression for  $f_{Af}$ , the first term, proportional to  $\log(r_b)$ , comes because our election for the term proportional to the divergence. The vector form factor,  $f_{Vf}$  can be written in terms of the other two form factors,

$$f_{Vf} = f_{Af} + f_{Tf}. \quad (\text{B.4})$$

In terms of these form factors the functions  $F_V$  and  $F_A$  that appear in eq. (2.13) are

$$F_V = \beta \left( \frac{(3 - \beta^2)}{2} f_{Vf} + \frac{3}{2} f_{Tf} \right), \quad (\text{B.5})$$

$$F_A = \beta^3 f_{Af}. \quad (\text{B.6})$$

The functions that come from real bremsstrahlung can be written as follows,

$$G_V = \beta \left( \frac{1}{2}(3 - \beta^2)G_P + G_{Vh} \right) , \quad (\text{B.7})$$

$$G_A = \beta \left( \beta^2 G_P + G_{Ah} \right) , \quad (\text{B.8})$$

where

$$G_P = G_{Ph} + 2f_\epsilon(1 + \log(\beta)) . \quad (\text{B.9})$$

The terms proportional to  $f_\epsilon$  come again from our choice of the coefficient of the divergence, and  $G_{Ph}$  is the finite part coming from the integration of the term proportional to  $h_p$  in the amplitude

$$G_{Ph} = \frac{C_F}{2\beta} \int_c^{1/c} dz g(z) \frac{1+z}{z} \log(g(z)^3 z(1+z)) . \quad (\text{B.10})$$

The result of the integration gives

$$G_{Ph} = C_F \left[ -2 \log \left( \frac{4\beta^3}{1-\beta^2} \right) + 2 - \frac{2+\beta^2}{\beta} \log(c) - \frac{1+\beta^2}{\beta} \left( \frac{1}{4} \log^2(c) + \frac{\pi^2}{3} - \text{Li}_2(c) - \text{Li}_2(c^2) - 3 \log(c) \log(1+c) \right) \right] . \quad (\text{B.11})$$

The functions  $G_{Vh}$  and  $G_{Ah}$  come from the integration of the  $h_V$  and  $h_A$  terms respectively

$$G_{Vh} = \frac{C_F}{4\beta} \int_c^{1/c} dz g(z)^2 \left( z + \frac{1}{z} \right) = -\frac{C_F}{8} \left( 9 + \beta^2 + \frac{9 - 2\beta^2 + \beta^4}{2\beta} \log(c) \right) , \quad (\text{B.12})$$

and

$$G_{Ah} = \frac{1}{2}(3 - \beta^2)G_{Vh} + (1 - \beta^2)\tilde{G}_{Ah} , \quad (\text{B.13})$$

where

$$\tilde{G}_{Ah} = \frac{C_F}{4\beta} \int_c^{1/c} dz g(z)^2 = \frac{C_F}{8} \left( 3 - \beta^2 + \frac{3 - 2\beta^2 - \beta^4}{2\beta} \log(c) \right) . \quad (\text{B.14})$$

## C Three-jet event rate functions

The functions  $H_V^{(0)}$  and  $H_A^{(0)}$ , which give the leading contribution to the three-jet decay rate in the EM algorithm, can be written in the following form

$$\begin{aligned} H_V^{(0)}(y_c, r_b) &= C_F \sum_{i=1,3} \theta_i \left[ \frac{(3 - \beta^2)}{2} K_S^i + K_V^i \right] \\ H_A^{(0)}(y_c, r_b) &= C_F \sum_{i=1,3} \theta_i \left[ \beta^2 K_S^i + \frac{(3 - \beta^2)}{2} K_V^i + (1 - \beta^2) K_A^i \right] . \end{aligned} \quad (\text{C.1})$$

with

$$\begin{aligned} \theta_1 &= \theta(\bar{y}_c - y_c) \\ \theta_2 &= -\theta(y_c - 2r_b)\theta(\bar{y}_c - y_c) \\ \theta_3 &= \theta(y_c - \bar{y}_c) \end{aligned}$$

and  $\bar{y}_c \approx \sqrt{r_b}(1 - \sqrt{r_b})$ . Here  $K_S^i$  corresponds to the soft part and  $K_{V(A)}^i$  to the vector (axial) hard part. These functions are given by

$$\begin{aligned}
K_S^1 &= 4y_c(z_\beta^{-1} - 1) - 2 \left( \frac{1 - \beta^2}{2} + 2y_c \right) \log(z_\beta) + 4\beta \log \left( \frac{z_\beta - c}{1 - z_\beta c} \right) \\
&+ (1 - \beta^2) \left[ 1 + z_\beta^{-1} - 2z_\beta + (z_\beta^{-1} - z_\beta) \log \left( \frac{y_c(1 + z_\beta)(1 + c)^2}{(z_\beta - c)(1 - z_\beta c)} \right) \right] \\
&+ 2(1 + \beta^2) \left[ \frac{1}{2} \log(z_\beta) \log \left( \frac{y_c^2(1 + c)^4}{z_\beta} \right) - \frac{\pi^2}{12} - \text{Li}_2(-z_\beta) - \text{Li}_2 \left( \frac{c}{z_\beta} \right) + \text{Li}_2(z_\beta c) \right]
\end{aligned} \tag{C.2}$$

$$\begin{aligned}
K_V^1 &= 1 + \frac{y_c^2(1 - z_\beta^{-2})}{2} - 2(1 + z_\beta)^{-1} + \frac{(1 - \beta^2)(3 + \beta^2)}{8}(z_\beta - z_\beta^{-1}) \\
&+ \frac{(1 - \beta^2)^2}{32}(z_\beta^{-2} - z_\beta^2) - \left( 1 + \frac{(1 - \beta^2)^2}{8} - y_c^2 \right) \log(z_\beta)
\end{aligned} \tag{C.3}$$

$$\begin{aligned}
K_A^1 &= -\frac{1}{2} + y_c^2(1 - z_\beta^{-1}) + \frac{(1 - \beta^2)^2}{16}(z_\beta^{-1} - z_\beta) + (1 + z_\beta)^{-1} \\
&+ \frac{(1 - \beta^2)(3 + \beta^2)}{8} \log(z_\beta)
\end{aligned} \tag{C.4}$$

$$\begin{aligned}
K_S^2 &= -2(1 + \beta^2 - 2y_c) \log(z_\alpha) + 4\beta \log \left( \frac{z_\alpha - c}{1 - z_\alpha c} \right) \\
&+ (1 - \beta^2)(z_\alpha^{-1} - z_\alpha) \left[ 2 + \log \left( \frac{(1 + \beta^2 - 2y_c)z_\alpha(1 + c)^2}{2(z_\alpha - c)(1 - cz_\alpha)} \right) \right] \\
&+ 2(1 + \beta^2) \left[ \log(z_\alpha) \log \left( \frac{(1 + \beta^2 - 2y_c)(1 + c)^2}{2} \right) - \text{Li}_2 \left( \frac{c}{z_\alpha} \right) + \text{Li}_2(cz_\alpha) \right]
\end{aligned} \tag{C.5}$$

$$\begin{aligned}
K_V^2 &= -(1 + \beta^2 - y_c)y_c \frac{(1 - z_\alpha)}{(1 + z_\alpha)} + \frac{(1 - \beta^2)^2}{32}(z_\alpha^{-2} - z_\alpha^2) \\
&+ \frac{(1 - \beta^2)(3 + \beta^2)}{8}(2 - z_\alpha^{-1} + z_\alpha - 4(1 + z_\alpha)^{-1}) \\
&- \left( \frac{(1 - \beta^2)(7 + \beta^2)}{8} + y_c + \beta^2 y_c - y_c^2 \right) \log(z_\alpha)
\end{aligned} \tag{C.6}$$

$$\begin{aligned}
K_A^2 &= \frac{(1 - \beta^2)^2}{16}(z_\alpha^{-1} - z_\alpha) + \frac{(1 + \beta^2 - y_c)y_c}{2} \frac{(1 - z_\alpha)}{(1 + z_\alpha)} \\
&+ \frac{(1 - \beta^2)(3 + \beta^2)}{8}(-1 + 2(1 + z_\alpha)^{-1} + \log(z_\alpha))
\end{aligned} \tag{C.7}$$

$$\begin{aligned}
K_S^3 &= -\frac{(1+\beta^2)\pi^2}{6} - \frac{(1-\beta^2-4\beta^2 z_\gamma)}{z_\gamma} \frac{(1-z_\gamma)}{(1+2z_\gamma)} + \frac{(1+3\beta^2-2(1-\beta^2)z_\gamma)}{(1+2z_\gamma)} \log(z_\gamma) \\
&+ (1+\beta^2) \left[ \log^2 \left( \frac{z_\gamma}{1+z_\gamma} \right) + 2\text{Li}_2 \left( \frac{z_\gamma}{1+z_\gamma} \right) \right]
\end{aligned} \tag{C.8}$$

$$K_V^3 = \frac{(1+\beta^2)^2}{8} \left( -\frac{3(1-z_\gamma^2)}{(1+2z_\gamma)^2} - \frac{2}{(1+2z_\gamma)} \log(z_\gamma) \right) \tag{C.9}$$

$$K_A^3 = \frac{(1+\beta^2)^2}{8} \left( \frac{1-z_\gamma}{1+2z_\gamma} \right)^2, \tag{C.10}$$

where we used the following notation,

$$\begin{aligned}
z_\alpha &= \frac{1}{2r_b} \left( y_c - \sqrt{y_c^2 - 4r_b^2} \right), \\
z_\beta &= \frac{1}{2r_b} \left( 1 - y_c - 2r_b - \sqrt{(1-y_c)^2 - 4r_b^2} \right), \\
z_\gamma &= \frac{y_c}{1-2r_b-2y_c}, \\
c &= \frac{1-\beta}{1+\beta}.
\end{aligned} \tag{C.11}$$

In the limit of massless quarks,  $r_b \rightarrow 0$ , from the functions  $H_V^{(0)}$  and  $H_A^{(0)}$  given above we obtain

$$H_V^{(0)}(y_c, r_b \rightarrow 0) = H_A^{(0)}(y_c, r_b \rightarrow 0) \rightarrow A^{(0)}, \tag{C.12}$$

Here the function  $A^{(0)}(y_c)$  is the known result [20, 21] for the JADE algorithm

$$\begin{aligned}
A^{(0)}(y_c) &= 2C_F \left[ -\frac{\pi^2}{3} + \frac{5}{2} - 6y_c - \frac{9}{2}y_c^2 + (3-6y_c) \log \left( \frac{y_c}{1-2y_c} \right) \right. \\
&\left. + 2 \log^2 \left( \frac{y_c}{1-y_c} \right) + 4\text{Li}_2 \left( \frac{y_c}{1-y_c} \right) \right].
\end{aligned} \tag{C.13}$$

The function  $A(y_c)$  given in refs. [20, 21] differs from our  $A^{(0)}(y_c)$  in a factor 2 because we chose a different normalization for it.

## D Angular distribution functions

The angular distribution studied in section 4 is given, in the massless case, by the function  $f_\vartheta(y_c)$ . In the JADE-type algorithms it can be written as follows

$$f_\vartheta(y_c) = C_F \sin(\vartheta) \sum_{i=1,2} \theta_i f_i(y_c), \tag{D.1}$$

where the  $\theta_i$  functions have the form

$$\begin{aligned}
\theta_1 &= \theta \left( \cos \vartheta + \frac{y_c}{(1-y_c)} \right) \theta \left( \frac{(1-6y_c+y_c^2)}{(1+y_c)^2} - \cos \vartheta \right), \\
\theta_2 &= \theta \left( -\frac{y_c}{(1-y_c)} - \cos \vartheta \right) \theta \left( \cos \vartheta + \frac{1-y_c}{1+y_c} \right),
\end{aligned}$$

and

$$\begin{aligned}
f_1(y_c) &= \frac{(1+b)^2}{b} \left[ \frac{y_c + 8b - 3}{4} \sqrt{(1-y_c)^2 - 4by_c} \right. \\
&\quad \left. - \log\left(\frac{x_1}{x_2}\right) + (1+b+2b^2) \log\left(\frac{b+x_1}{b+x_2}\right) \right] , \tag{D.2}
\end{aligned}$$

$$\begin{aligned}
f_2(y_c) &= \frac{(1+b)^2}{b} \left[ \frac{(y_c-b)(y_c^2 + 2y_c - 2by_c - 5b^2)}{4(b+y_c)} \right. \\
&\quad \left. - b(1+2b) \log\left(\frac{2b}{b+y_c}\right) - \log\left(\frac{1-b}{1-y_c}\right) \right] . \tag{D.3}
\end{aligned}$$

In these equations we defined

$$\begin{aligned}
b &= \frac{1 + \cos \vartheta}{1 - \cos \vartheta} , \\
x_1 &= \frac{1}{2} \left( 1 - y_c - \sqrt{(1-y_c)^2 - 4by_c} \right) , \\
x_2 &= \frac{1}{2} \left( 1 - y_c + \sqrt{(1-y_c)^2 - 4by_c} \right) .
\end{aligned}$$

# References

- [1] L3 Collaboration, B. Adeva, et al. , Phys. Lett. **B271** (1991) 461.
- [2] DELPHI Collaboration, P. Abreu, et al., Phys. Lett. **B307** (1993) 221.
- [3] OPAL Collaboration, R. Akers, et al., Z. für Physik C60 (1993) 397.
- [4] ALEPH Collaboration, “Test of flavour independence of the strong coupling constant”, Submitted to Glasgow Conference, 1994, ICHEP94, Ref. 0527.
- [5] J. Chrin, Proc. of the 28th Rencontre de Moriond, Les Arcs, Savoie, France, March 1993, pag. 313, ed. J. Trän Thanh Van.
- [6] J.A. Valls, “Determinación de la constante de acoplamiento fuerte para quarks  $b$ ,  $\alpha_s^b(M_Z)$ , con el detector DELPHI en LEP”, PhD. Thesis, Universitat de València, 1994.
- [7] See for example, P. Langacker and N. Polonsky, Phys.Rev. **D49** (1994) 1454, and references therein.
- [8] For a review see: L.J. Reinders, H. Rubinstein and S. Yazaki, Phys. Rep. **127** (1985) 1. J.H. Kuhn and P. M. Zerwas , Phys. Rep. **167** (1988) 321.
- [9] M.Shifman, A.I. Vainshtein, M.B. Voloshin and V.I. Zakharov Phys. Lett. **77B** (1978) 80; L.J. Reinders, H. Rubinstein and S. Yazaki, Phys. Lett. **103B** (1981) 63; T.H. Chang, K.J.F. Gaemers and W.L. van Neerven, Nucl. Phys. **B202** (1982) 407.
- [10] J. Schwinger, “Particles, Sources and Fields” (Addison-Wesley, Reading, Mass. 1973).
- [11] K.G. Chetyrkin and J.H. Kühn, Phys. Lett. **B248** (1990) 359.
- [12] K.G. Chetyrkin and A. Kwiatkowski, Phys. Lett. **B305** (1993) 285.
- [13] B.L. Ioffe, Phys. Lett. **78B** (1978) 277.
- [14] T.G. Rizzo, Phys. Rev. **D22** (1980) 2213; H.P. Nilles, Phys. Rev. Lett. **45** (1980) 319.
- [15] J. Jersák, E. Laermann and P.M. Zerwas, Phys. Rev. **D25** (1982) 1218; Erratum, Phys. Rev. **D36** (1987) 310.
- [16] A. Ballestrero, E. Maina, S. Moretti, Nucl. Phys. **B415** (1994) 265; A. Ballestrero, E. Maina, S. Moretti, Phys.Lett **B294** (1992) 425.
- [17] JADE Collaboration, W. Bartels et al., Z. für Physik **C33** (1986) 23.
- [18] R. Gastmans and R. Meuldermans, Nucl. Phys. **B63** (1973) 277; W.J. Marciano and A. Sirlin, Nucl. Phys. **B88** 1975 86; W.J. Marciano, Phys. Rev. **D12** (1975) 3861.
- [19] G. Sterman and S. Weinberg, Phys. Rev. Lett. **39** (1977) 1436.
- [20] S. Bethke et al., Nucl. Phys. **B370** (1992) 310.
- [21] Z. Kunszt , P. Nason, G. Marchesini and B.R. Webber, “Z Physics at LEP 1”, Vol 3: “Event Generators and Software”, CERN Yellow Report 89-08 (1989).



- [22] S. Catani et al. Phys. Lett. **B269** (1991) 432; N. Brown and W.J. Stirling, Z. Phys. **C53** (1992) 629.
- [23] A.A. Akhundov, D.Y. Bardin and T. Riemann, Nucl. Phys. **B276** (1986) 1; J. Bernabéu, A. Pich and A. Santamaria, Phys. Lett. **B200** (1988) 569; Nucl. Phys. **B363** (1991) 326; W. Beenakker and W. Hollik, Z. Phys. **C40** (1988) 141.
- [24] R.K. Ellis, D.A. Ross and A.E. Terrano, Nucl.Phys. **B178** (1981) 421; J.G. Körner and G.A. Schuler, Z. Phys. **26** (1985) 559; G. Kramer and B. Lampe, Z. Phys. **C34** (1987) 497; G.A. Schuler and J.G. Körner, Nucl.Phys. **B325** (1989) 557.
- [25] K. Hagiwara, T. Kuruma and Y. Yamada, Nucl. Phys. **B358** (1991) 80.
- [26] M. Bilenky, G. Rodrigo and A. Santamaria, work in progress.
- [27] F.A. Berends, G. Burgers and W.L. van Neerven, Nucl. Phys. **B297** (1988) 429; Erratum, Nucl. Phys. **B304** (1988) 921.
- [28] J. Fuster private communication.

Figure 1: Feynman diagrams contributing to the decay rates  $Z \rightarrow b\bar{b}$ ,  $Z \rightarrow b\bar{b}g$  at order  $\alpha_s$ .

Figure 2: The phase space for  $Z \rightarrow b\bar{b}g$  in the plane  $y_1$  and  $y_2$  with cuts ( $y_c = 0.04$  and  $y_c = 0.14$ ) for the different algorithms. The mass of the quark has been set to 10 GeV to enhance mass effects in the plot.

Figure 3: The ratios  $R_3^{bd}$  (see eq. (3.8)) for the four algorithms. Solid lines correspond to  $m_b = 5$  GeV, dashed lines correspond to  $m_b = 3$  GeV and dotted lines give our estimate of higher order corrections to the  $m_b = 5$  GeV curve. For the JADE algorithm we have also included the results of the analysis of the data collected during 1990-1991 by the DELPHI group [2].

Figure 4: The functions  $B_V^{(0)}/A^{(0)}$  and  $B_A^{(0)}/A^{(0)}$  for the four algorithms. Dashed lines for  $m_b = 3$  GeV, dotted lines for  $m_b = 5$  GeV and solid lines for our three-parameter fit, eq. (3.11).

Figure 5: Normalized angular distributions (eq. (4.4)) with respect to the angle formed between the quark and the gluon jets for the massless case for JADE-type and DURHAM algorithms. Solid line for  $y_c = 0.02$ , dashed line for  $y_c = 0.04$ , dotted line for  $y_c = 0.06$  and dash-dotted line for  $y_c = 0.08$

Figure 6: The ratios of angular distributions  $R_\theta^{bd}$  (see eq. (4.3)) for  $y_c = 0.04$  for the different algorithms. Solid line for  $m_b = 5$  GeV and dashed line for  $m_b = 3$  GeV.

# Three-jet production at LEP and the bottom quark mass

**Mikhail Bilenky**<sup>\*)</sup>

DESY-IfH, Platanenallee 6, 15738 Zeuthen, Germany

**Germán Rodrigo**

Dept. de Física Teòrica, Univ. de València,  
E-46100 Burjassot (València), Spain

and

**Arcadi Santamaria**<sup>\*\*)</sup>

TH Division, CERN, 1211 Genève 23, Switzerland

## Abstract

We consider the possibility of extracting the bottom quark mass from LEP data. The inclusive decay rate for  $Z \rightarrow b\bar{b} + \dots$  is obtained at order  $\alpha_s$  by summing up the one-loop two-parton decay rate to the tree-level three-parton rate. We calculate the decay width of the  $Z$ -boson into two and three jets containing the  $b$ -quark including complete quark mass effects. In particular, we give analytic results for a slight modification of the JADE clustering algorithm. We also study the angular distribution with respect to the angle formed between the gluon and the quark jets, which has a strong dependence on the quark mass. The impact of higher order QCD corrections on these observables is briefly discussed. Finally, we present numerical results for some popular jet-clustering algorithms and show that, indeed, these three-jet observables are very sensitive to the  $b$ -quark mass and well suited for its determination at LEP.

CERN-TH.7419/94

October 11, 1994

---

<sup>\*)</sup> On leave of absence from the Joint Institute for Nuclear Research, Dubna, Russia.

<sup>\*\*)</sup>  On leave of absence from Departament de Física Teòrica, Universitat de València, and IFIC, València, Spain.

# 1 Introduction

In the Standard Model of electroweak interactions all fermion masses are free parameters and their origin, although linked to the spontaneous symmetry breaking mechanism, remains secret. Masses of charged leptons are well measured experimentally and neutrino masses, if they exist, are also bounded. In the case of quarks the situation is more complicated because free quarks are not observed in nature. Therefore, one can only get some indirect information on the values of the quark masses. For light quarks ( $m_q < 1$  GeV, the scale at which QCD interactions become strong), that is, for  $u$ -,  $d$ - and  $s$ -quarks, one can define the quark masses as the parameters of the Lagrangian that break explicitly the chiral symmetry of the massless QCD Lagrangian. Then, these masses can be extracted from a careful analysis of meson spectra and meson decay constants. For heavy quarks ( $c$ - and  $b$ -quarks) one can obtain the quark masses from the known spectra of the hadronic bound states by using, e.g., QCD sum rules or lattice calculations. However, since the strong gauge coupling constant is still large at the scale of heavy quark masses, these calculations are plagued by uncertainties and nonperturbative effects.

It would be very interesting to have some experimental information on the quark masses obtained at much larger scales where a perturbative quark mass definition can be used and, presumably, non-perturbative effects are negligible. The measurements at LEP will combine this requirement with very high experimental statistics.

The effects of quark masses can be neglected for many observables in LEP studies, as usually quark masses appear in the ratio  $m_q^2/m_Z^2$ . For the bottom quark, the heaviest quark produced at LEP, and taking a  $b$ -quark mass of about 5 GeV this ratio is 0.003, even if the coefficient in front is 10 we get a correction of about 3%. Effects of this order are measurable at LEP, however, as we will see later, in many cases the actual mass that should be used in the calculations is the *running* mass of the  $b$ -quark computed at the  $m_Z$  scale:  $\bar{m}_b(m_Z) \approx 3$  GeV rendering the effect below the LEP precision for most of the observables.

While this argument is correct for total cross sections for production of  $b$ -quarks it is not completely true for quantities that depend on other variables. In particular it is not true for jet cross sections which depend on a new variable,  $y_c$  (the jet-resolution parameter that defines the jet multiplicity) and which introduces a new scale in the analysis,  $E_c = m_Z \sqrt{y_c}$ . Then, for small values of  $y_c$  there could be contributions coming like  $m_b^2/E_c^2 = (m_b/m_Z)^2/y_c$  which could enhance the mass effect considerably. In addition mass effects could also be enhanced by logarithms of the mass. For instance, the ratio of the phase space for two massive quarks and a gluon to the phase space for three massless particles is  $1 + 8(m_q/m_Z)^2 \log(m_q/m_Z)$ . This represents a 7% effect for  $m_q = 5$  GeV and a 3% effect for  $m_q = 3$  GeV.

The high precision achieved at LEP makes these effects relevant. In fact, they have to be taken into account in the test of the flavour independence of  $\alpha_s(m_Z)$  [1–5]. In particular it has been shown [6] that the biggest systematic error in the measurement of  $\alpha_s^b(m_Z)$  ( $\alpha_s$  obtained from  $b\bar{b}$ -production at LEP from the ratio of three to two jets) comes from the uncertainties in the estimate of the quark mass effects. This in turn means that mass effects have already been seen. Now one can reverse the question and ask about the possibility of measuring the mass of the bottom quark,  $m_b$ , at LEP by assuming the flavour universality of the strong interactions.

Such a measurement will also allow to check the running of  $\bar{m}_b(\mu)$  from  $\mu = m_b$  to  $\mu = m_Z$  as has been done before for  $\alpha_s(\mu)$ . In addition  $\bar{m}_b(m_Z)$  is the crucial input parameter in the analysis of the unification of Yukawa couplings predicted by many grand unified theories and which has attracted much attention in the last years [7].

The importance of quark mass effects in  $Z$ -boson decays has already been discussed in the literature [8]. The complete order  $\alpha_s$  results for the inclusive decay rate of  $Z \rightarrow b\bar{b} + b\bar{b}g + \dots$

can be found<sup>1</sup> in [9]. The leading quark mass effects for the inclusive  $Z$ -width are known to order  $\alpha_s^3$  for the vector part [11] and to order  $\alpha_s^2$  for the axial-vector part [12]. Quark mass effects for three-jet final states in the process  $e^+e^- \rightarrow q\bar{q}g$  were considered first in [13] for the photonic channel and extended later to the  $Z$  channel in [14] and [15]. Recently [16] calculations of the three-jet event rates, including mass effects, were done for the most popular jet clustering algorithms using the Monte Carlo approach.

In this paper we will discuss the possibility of measuring the  $b$ -quark mass at LEP, in particular, we study bottom quark mass effects in  $Z$  decays into two and three jets. In section 2 we calculate the inclusive decay rate  $Z \rightarrow b\bar{b} + b\bar{b}g + \dots$  at order  $\alpha_s$  by summing one-loop virtual corrections to  $Z \rightarrow b\bar{b}$  and the real gluon bremsstrahlung contribution. Dimensional continuation is used to regularize both infrared (IR) and ultraviolet (UV) divergences. Phase space integrations are also done in  $D$  dimensions. This calculation allows us to understand the details of the cancellation of IR divergences and how some, potentially large, logarithms of the quark mass are absorbed in the running quark mass  $\bar{m}_b(m_Z)$ . In section 3 we calculate analytically the two and three-jet event rates in terms of the jet-resolution parameter  $y_c$  and the mass of the quark for a slight modification of the well-known JADE algorithm [17] suitable for analytic calculations with massive quarks. We also present numerical results for this scheme and for some of the most popular jet-clustering algorithms (DURHAM ( $K_T$ ), JADE and E), estimate higher order contributions and compare with experimental results obtained by the DELPHI Collaboration [2] for 1990-1991 data. If the gluon jet can be identified with good efficiency a very interesting observable, which strongly depends on the quark mass, is the angular distribution with respect to the angle formed between the quark and the gluon jets. This distribution is calculated for massless quarks in section 4: analytically for JADE-type algorithms and numerically for the DURHAM algorithm. We also compute numerically the ratio of massive to massless angular distributions for the four jet-clustering algorithms. In section 5 we summarize the results obtained in the paper and comment on the possibility of using them to measure the  $b$ -quark mass in LEP experiments. Finally in the four appendices we collect all the functions and formulae needed in the body of the paper.

## 2 The inclusive decay rate $Z \rightarrow b\bar{b}$

The main purpose of this paper is to investigate  $b$ -quark mass effects in  $Z$  decays into two and three jets. Since at order  $\alpha_s$  the inclusive decay rate  $Z \rightarrow b\bar{b} + \dots$  is given by the sum of the two- and three-jet decay widths we will start by studying this quantity.

To calculate the total decay rate to order  $\alpha_s$ , one has to sum up the virtual one-loop gluonic corrections to the  $Z \rightarrow b\bar{b}$  with the real gluon bremsstrahlung. Both contributions are separately infrared divergent for massless gluons, therefore, some regularization method for the IR divergences is needed. The sum is, however, IR finite.

Since there are many subtleties in this calculation, we sketch it in this section. Both processes,  $Z \rightarrow b\bar{b}$  at one loop and  $Z \rightarrow b\bar{b}g$ , are calculated in arbitrary dimension  $D = 4 - 2\epsilon$  and dimensional regularization is used to regularize the IR divergences [18]. At order  $\alpha_s$  and for massive quarks all IR divergences appear as simple poles  $1/\epsilon$ . We show how the divergences cancel in the sum and obtain the total inclusive rate.

The first step is to compute the decay width  $Z \rightarrow b\bar{b}$  at tree-level in dimension  $D$ . Since there are no IR divergences in this case it is not necessary to do the calculations in arbitrary

---

<sup>1</sup>The order  $\alpha_s$  corrections to the vector part, including the complete mass dependences, were already known from QED calculations [10].

space-time dimensions. However, there are IR divergences at the one-loop level and  $\epsilon$  factors could lead to finite contributions when multiplied by the divergent terms.

The amplitude for the decay  $Z \rightarrow b\bar{b}$  in  $D$  dimensions is

$$T_b^{(0)} = \mu^\epsilon \frac{g}{4c_W} \bar{u}_1 \gamma_\mu (g_V + g_A \gamma_5) v_2 \epsilon^\mu(q), \quad (2.1)$$

where the factor  $\mu^\epsilon$  has been included to make the gauge weak coupling  $g$  dimensionless in  $D$  dimensions;  $u_1$  and  $v_2$  are short-hand notations for the quark (antiquark) spinors,  $u_1 = u(p_1)$  and  $v_2 = v(p_2)$ ,  $\epsilon^\mu(q)$  stands for the polarization vector of the  $Z$ -boson and  $g_V$  ( $g_A$ ) are the vector (axial-vector) neutral current couplings of the quarks in the Standard Model. At tree level and for the  $b$ -quark we have

$$g_V = -1 + \frac{4}{3}s_W^2, \quad g_A = 1. \quad (2.2)$$

Here we denote by  $c_W$  and  $s_W$  the cosine and the sine of the weak mixing angle.

Taking the square of the amplitude, averaging over initial state polarizations, summing over final state polarizations, and adding the phase space factor for the two-body decay given in appendix A [18] we obtain the following decay width in  $D$  dimensions,

$$\Gamma_b^{(0)} = C_b A_b \beta^{1-2\epsilon}, \quad (2.3)$$

with

$$C_b = m_Z \frac{g^2}{c_W^2 64\pi} \frac{\Gamma(1-\epsilon)}{\Gamma(2-2\epsilon)} \left( \frac{m_Z^2}{4\pi\mu^2} \right)^{-\epsilon}, \quad (2.4)$$

and

$$A_b = \frac{1}{2}(3 - \beta^2 - 2\epsilon)g_V^2 + \beta^2(1 - \epsilon)g_A^2. \quad (2.5)$$

In these expressions  $\beta$  is the relative velocity of the produced quarks

$$\beta = \sqrt{1 - 4r_b}, \quad r_b = \frac{m_b^2}{m_Z^2}. \quad (2.6)$$

At the one-loop level (see diagrams in fig. 1b), and after renormalization of the UV divergences<sup>2</sup>, the amplitude can be conveniently parameterized in terms of three form factors,  $f_V$ ,  $f_A$  and  $f_T$ ,

$$T_b = \mu^\epsilon \frac{g}{4c_W} \bar{u}_1 \left( g_V \left( \left( 1 + \frac{1}{2}C_g f_V \right) \gamma_\mu + i \frac{1}{2}C_g f_T \frac{\sigma_{\mu\nu} q^\nu}{2m_b} \right) + g_A \left( 1 + \frac{1}{2}C_g f_A \right) \gamma_\mu \gamma_5 \right) v_2 \epsilon^\mu(q), \quad (2.7)$$

where  $C_g$  is defined as follows,

$$C_g = \frac{\alpha_s}{\pi} \left( \frac{m_Z^2}{4\pi\mu^2} \right)^{-\epsilon} \frac{1}{\Gamma(1-\epsilon)}. \quad (2.8)$$

Here and below we will conventionally use  $\alpha_s = \alpha_s(m_Z)$  to denote the value of the running strong coupling at the  $m_Z$ -scale.

---

<sup>2</sup>Note that conserved currents or partially conserved currents as the vector and axial currents do not get renormalized. Therefore, all UV divergences cancel when one sums properly self-energy and vertex diagrams. The remaining poles in  $\epsilon$  correspond to IR divergences. One can see this by separating carefully the poles corresponding to UV divergences from the poles corresponding to IR divergences.

The form factors,  $f_V$ ,  $f_A$  and  $f_T$ , are related by

$$f_V = f_A + f_T . \quad (2.9)$$

The two functions,  $f_V$  and  $f_A$ , contain an IR divergence, while  $f_T$  is finite. Separating the divergent parts, we can rewrite the real parts of the form factors as follows (at order  $\alpha_s$  the imaginary parts will not contribute)

$$\text{Re} \{f_V\} = -\frac{1}{\epsilon} f_\epsilon + f_{Vf} , \quad (2.10)$$

$$\text{Re} \{f_A\} = -\frac{1}{\epsilon} f_\epsilon + f_{Af} , \quad (2.11)$$

$$\text{Re} \{f_T\} \equiv f_{Tf} , \quad (2.12)$$

where all functions  $f_\epsilon$ ,  $f_{Vf}$ ,  $f_{Af}$  and  $f_{Tf}$  are given in appendix B. Note that, as expected, the IR divergent part of the amplitude is proportional to the tree-level amplitude eq. (2.1). As the IR divergence manifests itself as a single pole in  $\epsilon$ , clearly, we only need to keep everywhere terms linear in  $\epsilon$ .

From the amplitude (2.7) we obtain the one-loop corrected width in  $D$  dimensions

$$\Gamma_b^D = \Gamma_b^{(0)} + \Gamma_b^{(1)} ,$$

with

$$\Gamma_b^{(1)} = -C_g f_\epsilon \frac{1}{\epsilon} \Gamma_b^{(0)} + C_b C_g (g_V^2 F_V + g_A^2 F_A) , \quad (2.13)$$

where the finite functions  $F_V$  and  $F_A$  are given in appendix B in terms of the form factors and  $\Gamma_b^{(0)}$  is given by eq. (2.3)

The  $O(\alpha_s)$  result, eq. (2.13), is divergent for  $\epsilon \rightarrow 0$  because the IR divergences associated with massless gluons running in the loops. To get a finite answer at this order we also need to include gluon bremsstrahlung from the quarks. This has to be computed by working in  $D$  dimensions.

The amplitude for the process  $Z \rightarrow b\bar{b}g$  (the two corresponding diagrams are given in fig. 1c) can be written as

$$\begin{aligned} T_{bg} = & \mu^{2\epsilon} \frac{g}{4c_W} g_s \bar{u}_1 \left( \frac{\gamma_\nu (\not{p}_1 + \not{k} + m_b) \gamma_\mu (g_V + g_A \gamma_5)}{2(p_1 k)} \right. \\ & \left. + \frac{\gamma_\mu (g_V + g_A \gamma_5) (-\not{p}_2 - \not{k} + m_b) \gamma_\nu}{2(p_2 k)} \right) \frac{\lambda^a}{2} v_2 \epsilon_a^\nu(k) \epsilon^\mu(q) . \end{aligned} \quad (2.14)$$

Here  $\lambda^a$  are the Gell-Mann  $SU(3)$  matrices, and  $\epsilon_a^\nu(k)$  is the gluon polarization vector.

The square of the amplitude, in dimension  $D$ , gives a rather involved expression that can be conveniently simplified when one realizes that the most divergent part of it factorizes completely, even in  $D$  dimensions, due to the factorization theorems for soft and collinear divergences.

Adding the three-body phase space (see appendix A) we find that the decay width of  $Z \rightarrow b\bar{b}g$  in  $D$  dimensions can be written as

$$\Gamma_{bg} = C_b C_g C_F \int dy_1 dy_2 \theta(h_p) h_p^{-\epsilon} A_{bg} , \quad (2.15)$$

where  $C_F = 4/3$  is the  $SU(3)$  group factor,  $y_1$  and  $y_2$  are defined in terms of the energy fractions of the two outgoing quarks

$$y_1 = 2(p_1 k)/m_Z^2 = 1 - 2E_2/m_Z , \quad y_2 = 2(p_2 k)/m_Z^2 = 1 - 2E_1/m_Z \quad (2.16)$$



and  $A_{bg}$  comes from the square of the matrix element,

$$A_{bg} = A_b \frac{h_p}{y_1^2 y_2^2} + g_V^2 h_V + g_A^2 h_A . \quad (2.17)$$

Here  $A_b$  is the same combination of couplings and masses that appears in the tree-level decay width to two quarks, eq. (2.5), and the function  $h_p$  is given by

$$h_p = y_1 y_2 (1 - y_1 - y_2) - r_b (y_1 + y_2)^2 , \quad (2.18)$$

and it is exactly the same function that defines the phase space available for the three-body decay (see eq. (2.15) and appendix A). After phase space integration this term will contain an IR divergence which comes from the singularity at  $y_1 = y_2 = 0$ .

The functions  $h_V$  and  $h_A$  describe the vector and the axial-vector parts of the remainder of the square of the amplitude which do not generate any IR divergence. In the limit  $\epsilon = 0$  they are given by:

$$h_V = \frac{1}{2} \left( \frac{y_2}{y_1} + \frac{y_1}{y_2} \right) , \quad (2.19)$$

$$h_A = (1 + 2r_b) h_V + 2r_b . \quad (2.20)$$

To perform the phase space integration it is convenient to change variables as follows

$$\begin{aligned} y_1 &= g(z)w , \\ y_2 &= g(z)zw , \end{aligned}$$

with

$$g(z) = \frac{z - r_b(1+z)^2}{z(1+z)} = \frac{1}{(1+c)^2} \frac{(z-c)(1-cz)}{z(1+z)} \quad (2.21)$$

and

$$c = \frac{1-\beta}{1+\beta} . \quad (2.22)$$

Then, both  $h_V$  and  $h_A$  only depend on the variable  $z$ , and the function  $h_p$ , which defines phase space and appears explicitly in eq. (2.17), factorizes completely

$$h_p = g(z)^3 z(1+z)w^2(1-w) . \quad (2.23)$$

The function  $g(z)$  has zeros at  $z_1 = c$  and  $z_2 = 1/c$ . As phase space is defined by  $h_p > 0$  we obtain that the phase space in terms of the new variables is given by

$$c < z < 1/c \quad \text{and} \quad 0 < w < 1 . \quad (2.24)$$

After this change of variables eq. (2.15) can be rewritten as

$$\Gamma_{bg} = C_b C_g C_F \int_c^{1/c} dz g(z)^2 \int_0^1 dw w h_p^{-\epsilon} A_{bg} . \quad (2.25)$$

Now the  $w$  integration is very simple and leads to Beta functions. For the integration of the term of the amplitude proportional to  $A_b$  (see eq. (2.17)) we get

$$\int_c^{1/c} dz \int_0^1 dw h_p^{1-\epsilon} \frac{1}{g(z)^2 z^2 w^3} = B(-2\epsilon, 2-\epsilon) \int_c^{1/c} dz \frac{1}{g(z)^2 z^2} \left( g(z)^3 z(1+z) \right)^{1-\epsilon} , \quad (2.26)$$

where the function  $B(-2\epsilon, 2 - \epsilon)$  has a single pole in  $\epsilon = 0$ . In this way, all the divergent behaviour has been factorized in the Beta function. Then, to perform the  $z$  integration we can expand the integrant for small  $\epsilon$  and keep only terms linear in  $\epsilon$ . The integrations can be easily performed and the results written in terms of logarithms and dilogarithmic functions. The rest of the integrals do not lead to any divergence and can be done, without problem, putting  $\epsilon$  equal to zero.

After phase space integration, the decay width for  $Z \rightarrow b\bar{b}g$  can be written in the following form

$$\Gamma_{bg} = C_g f_\epsilon \frac{1}{\epsilon} \Gamma_b^{(0)} + C_b C_g \left( g_V^2 G_V + g_A^2 G_A \right), \quad (2.27)$$

where the first term contains the IR divergent part and the IR finite functions  $G_V$  and  $G_A$  are given in appendix B.

The IR divergent part of eq. (2.27) is identical, but with reversed sign, to the one obtained for  $\Gamma_b^{(1)}$ , therefore in the sum they will cancel, as it should be:

$$\Gamma_b = \Gamma_b^{(0)} + \Gamma_b^{(1)} + \Gamma_{bg} = \Gamma_b^{(0)} + C_b C_g \left( g_V^2 T_V + g_A^2 T_A \right), \quad (2.28)$$

with

$$T_V = F_V + G_V, \quad (2.29)$$

$$T_A = F_A + G_A. \quad (2.30)$$

From the results of the appendix B we can easily obtain the limit of these functions for small quark masses,  $m_b \ll m_Z$  ( $r_b \ll 1$ )

$$T_V \approx 1 + 12r_b, \quad (2.31)$$

$$T_A \approx 1 - 6r_b(2 \log r_b + 1). \quad (2.32)$$

If we plug this result into eq. (2.28) we obtain the well-known result [11]

$$\Gamma_b = m_Z \frac{g^2}{c_W^2 64\pi} \left[ g_V^2 \left( 1 + \frac{\alpha_s}{\pi} (1 + 12r_b) \right) + g_A^2 \left( 1 - 6r_b + \frac{\alpha_s}{\pi} (1 - 6r_b(2 \log r_b + 1)) \right) \right]. \quad (2.33)$$

It is interesting to note the presence of the large logarithm,  $\log(m_b^2/m_Z^2)$ , proportional to the quark mass in the axial part of the QCD corrected width, eq. (2.33). The mass that appears in all above calculations should be interpreted as the perturbative *pole* mass of the quark. But in principle the expression (2.33) could also be written in terms of the so-called *running* quark mass at the  $m_Z$  scale by using

$$m_b^2 = \bar{m}_b^2(m_Z) \left[ 1 + 2 \frac{\alpha_s}{\pi} \left( \log \left( \frac{m_Z^2}{m_b^2} \right) + \frac{4}{3} \right) \right]. \quad (2.34)$$

Then, we see that all large logarithms are absorbed in the running of the quark mass from the  $m_b$  scale to the  $m_Z$  scale [11] and we have

$$\Gamma_b = m_Z \frac{g^2}{c_W^2 64\pi} \left[ g_V^2 \left( 1 + \frac{\alpha_s}{\pi} (1 + 12\bar{r}_b) \right) + g_A^2 \left( 1 - 6\bar{r}_b + \frac{\alpha_s}{\pi} (1 - 22\bar{r}_b) \right) \right], \quad (2.35)$$

where  $\bar{r}_b = \bar{m}_b^2(m_Z)/m_Z^2$ .

This result means that the bulk of the QCD corrections depending on the mass could be accounted for by using tree-level expressions for the decay width but interpreting the quark

mass as the running mass at the  $m_Z$  scale. On the other hand, since  $\bar{m}_b(m_Z) \approx 3$  GeV is much smaller than the pole mass,  $m_b \approx 5$  GeV, it is clear that the quark mass corrections are much smaller than expected from the naïve use of the tree-level result with  $m_b \approx 5$  GeV, which would give mass corrections at the 1.8% level while in fact, once QCD corrections are taken into account, the mass corrections are only at the 0.7% level.

The final results of this section are well known but we find they could illuminate the discussion of mass effects in the two- and three-jet event rates and in the angular distribution with respect to the angle formed between the quark and gluon jets. Moreover the intermediate results of this section will be used in the rest of the paper.

### 3 Two- and three-jet event rates

According to our current understanding of the strong interactions, coloured partons, produced in hard processes, are hadronized and, at experiment, one only observes colourless particles. It is known empirically that, in high energy collision, final particles group in several clusters by forming energetic jets, which are related to the primordial partons. Thus, in order to compare theoretical predictions with experiments, it is necessary to define precisely what is a jet in both, parton level calculations and experimental measurements.

As we have seen in the previous section, at order  $\alpha_s$ , the decay widths of  $Z$  into both two and three partons are IR divergent. The two-parton decay rate is divergent due to the massless gluons running in the loops. The  $Z$ -boson decay width into three-partons has an IR divergence because massless gluons could be radiated with zero energy. The sum, however, is IR finite. Then it is clear that at the parton-level one can define an IR finite *two-jet decay rate*, by summing the two-parton decay rate and the IR divergent part of the three-parton decay width, e.g. integrated over the part of the phase space which contains soft gluon emission [19]. The integral over the rest of the phase space will give the *three-jet decay rate*. Thus we need to introduce a “resolution parameter” in the theoretical calculations in order to define IR-safe observables. Obviously, the resolution parameter, which defines the two- and the three-jet parts of the three-parton phase space should be related to the one used in the process of building jets from real particles.

In the last years the most popular definitions of jets are based on the so-called jet clustering algorithms. These algorithms can be applied at the parton level in the theoretical calculations and also to the bunch of real particles observed at experiment. It has been shown that, for some of the algorithms, the passage from partons to hadrons (hadronization) does not change much the behaviour of the observables [20], thus allowing to compare theoretical predictions with experimental results. In what follows we will use the word particles for both partons and real particles.

In the jet-clustering algorithms jets are defined as follows: starting from a bunch of particles with momenta  $p_i$  one computes, for example, a quantity like

$$y_{ij} = 2 \frac{E_i E_j}{s} (1 - \cos \theta_{ij})$$

for all pairs  $(i, j)$  of particles. Then one takes the minimum of all  $y_{ij}$  and if it satisfies that it is smaller than a given quantity  $y_c$  (the resolution parameter, y-cut) the two particles which define this  $y_{ij}$  are regarded as belonging to the same jet, therefore, they are recombined into a new pseudoparticle by defining the four-momentum of the pseudoparticle according to some rule, for example

$$p_k = p_i + p_j .$$

Algorithm	Resolution	Combination
EM	$2(p_i p_j)/s$	$p_k = p_i + p_j$
JADE	$2(E_i E_j)/s (1 - \cos \vartheta_{ij})$	$p_k = p_i + p_j$
E	$(p_i + p_j)^2/s$	$p_k = p_i + p_j$
DURHAM	$2 \min(E_i^2, E_j^2)/s (1 - \cos \vartheta_{ij})$	$p_k = p_i + p_j$

Table 1: The jet-clustering algorithms

After this first step one has a bunch of pseudoparticles and the algorithm can be applied again and again until all the pseudoparticles satisfy  $y_{ij} > y_c$ . The number of pseudoparticles found in the end is the number of jets in the event.

Of course, with such a jet definition the number of jets found in an event and its whole topology will depend on the value of  $y_c$ . For a given event, larger values of  $y_c$  will result in a smaller number of jets. In theoretical calculations one can define cross sections or decay widths into jets as a function of  $y_c$ , which are computed at the parton level, by following exactly the same algorithm. This procedure leads automatically to IR finite quantities because one excludes the regions of phase space that cause trouble. The success of the jet-clustering algorithms is due, mainly, to the fact that the cross sections obtained after the hadronization process agree quite well with the cross-sections calculated at the parton level when the same clustering algorithm is used in both theoretical predictions and experimental analyses.

There are different successful jet-clustering algorithms and we refer to refs. [20, 21] for a detailed discussion and comparison of these algorithms in the case of massless quarks.

In the rest of the paper we will use the four jet-clustering algorithms listed in the table 1, where  $\sqrt{s}$  is the total centre of mass energy. In addition to the well-known JADE, E and DURHAM algorithms we will use a slight modification of the JADE scheme particularly useful for analytical calculations with massive quarks. It is defined by the two following equations

$$y_{ij} = 2 \frac{p_i p_j}{s}$$

and

$$p_k = p_i + p_j$$

We will denote this algorithm as the EM scheme. For massless particles and at the lowest order E, JADE and EM give the same answers. However already at order  $\alpha_s^2$  they give different answers since after the first recombination the pseudoparticles are not massless anymore and the resolution functions are different.

For massive quarks the three algorithms, E, JADE and EM are already different at order  $\alpha_s$ . The DURHAM ( $K_T$ ) algorithm, which has been recently considered in order to avoid exponentiation problems present in the JADE algorithm [22, 20], is of course completely different from the other algorithms we use, both in the massive and the massless cases.

In figure 2 we plotted the phase-space for two values of  $y_c$  ( $y_c = 0.04$  and  $y_c = 0.14$ ) for all four schemes (the solid line defines the whole phase space for  $Z \rightarrow q\bar{q}g$  with  $m_q = 10$  GeV).

There is an ongoing discussion on which is the best algorithm for jet clustering in the case of massless quarks. The main criteria followed to choose them are based in two requirements:

1. Minimize higher order corrections.

## 2. Keep the equivalence between parton and hadronized cross sections.

To our knowledge no complete comparative study of the jet-clustering algorithms has been done for the case of massive quarks. The properties of the different algorithms with respect to the above criteria can be quite different in the case of massive quarks from those in the massless case. The first one because the leading terms containing double-logarithms of  $y$ -cut ( $\log^2(y_c)$ ) that appear in the massless calculation (at order  $\alpha_s$ ) and somehow determine the size of higher order corrections are substituted in the case of massive quarks by single-logarithms of  $y_c$  times a logarithm of the quark mass. The second one because hadronization corrections for massive quarks could be different from the ones for massless quarks.

Therefore, we will not stick to any particular algorithm but rather present results and compare them for all the four algorithms listed in the table 1.

### 3.1 The analytic calculation for the EM scheme

Here we calculate analytically, at leading order, the three-jet decay rate of the  $Z$ -boson by using the EM clustering algorithm.

At the parton level the two-jet region in the decay  $Z \rightarrow b\bar{b}g$  is given, in terms of the variables  $y_1$  and  $y_2$ , by the following conditions:

$$y_1 < y_c \quad \text{or} \quad y_2 < y_c \quad \text{or} \quad 1 - 2r_b - y_1 - y_2 < y_c . \quad (3.1)$$

This region contains the IR singularity,  $y_1 = y_2 = 0$  and the rate obtained by the integration of the amplitude over this part of the phase space should be added to the one-loop corrected decay width for  $Z \rightarrow b\bar{b}$ . The sum of these two quantities is of course IR finite and it is the so-called two-jet decay width at order  $\alpha_s$ . The integration over the rest of the phase space defines the three-jet decay width at the leading order. It is obvious that the sum of the two-jet and three-jet decay widths is independent of the resolution parameter  $y_c$ , IR finite and given by the quantity  $\Gamma_b = \Gamma(Z \rightarrow b\bar{b} + b\bar{b}g + \dots)$  calculated in section 2. Therefore we have

$$\Gamma_b = \Gamma_{2j}^b(y_c) + \Gamma_{3j}^b(y_c) + \dots .$$

Clearly, at order  $\alpha_s$ , knowing  $\Gamma_b$  and  $\Gamma_{3j}^b(y_c)$  we can obtain  $\Gamma_{2j}^b(y_c)$  as well.

The calculation of  $\Gamma_{3j}^b(y_c)$  at order  $\alpha_s$  is a tree-level calculation and does not have any IR problem since the soft gluon region has been excluded from phase space. Therefore the calculation can be done in four dimensions without trouble.

We will start with equation (2.15) taking  $\epsilon = 0$  and with the phase space constrained by the cuts defined in eq. (3.1).

$$\Gamma_{3j}^b = \left( C_b C_g C_F \int dy_1 dy_2 \theta_{PS} \theta_c A_{bg} \right)_{\epsilon=0} , \quad (3.2)$$

where the  $\theta$  function

$$\theta_{PS} = \theta(h_p) \quad (3.3)$$

gives the whole phase space, and the product of  $\theta$  functions

$$\theta_c = \theta(y_2 - y_c) \theta(y_1 - y_c) \theta(1 - 2r_b - y_1 - y_2 - y_c) \quad (3.4)$$

introduces the appropriate cuts for the EM scheme. The square of the amplitude,  $A_{bg}$ , is given in eq. (2.17). The phase space and the cuts are represented in the first plot of fig. 2.

Depending on the value of  $y_c$  the limits of integration are different, there are three cases which correspond to three different topologies of the overlapping of the phase space and the area defined by the cuts:

$$\begin{aligned} y_c &< 2r_b \\ 2r_b &< y_c < \bar{y}_c \\ \bar{y}_c &< y_c \end{aligned} , \quad (3.5)$$

where  $\bar{y}_c = \sqrt{r_b}(1 - \sqrt{r_b}) + O(r_b^2\sqrt{r_b})$  is given by a solution of the following equation

$$4(1 - 2y_c - 2r_b)^2(y_c^2 + 4r_b) = y_c^2(2 - y_c - 8r_b)^2. \quad (3.6)$$

Since the integrant is symmetric under the exchange  $y_1 \leftrightarrow y_2$  we can restrict the region of integration to the region  $y_1 > y_2$  (multiplying the result by a factor 2). In addition it is useful to change variables as before,  $y_2 = zy_1$ . We will not discuss the technical details of the calculation here; all of the integrals can be reduced to logarithmic and dilogarithmic functions and the final result can be written in the following form

$$\Gamma_{3j}^b = C_b C_g \left( g_V^2 H_V^{(0)}(y_c, r_b) + g_A^2 H_A^{(0)}(y_c, r_b) \right) , \quad (3.7)$$

where the superscript  $(0)$  in the functions  $H_{V(A)}^{(0)}(y_c, r_b)$  reminds us that this is only the lowest order result. Analytical expressions for the functions  $H_V^{(0)}(y_c, r_b)$  and  $H_A^{(0)}(y_c, r_b)$  are given in appendix C. Obviously, the general form (3.7) is independent of what particular jet-clustering algorithm has been used.

In the limit of zero masses,  $r_b = 0$ , chirality is conserved and the two functions  $H_V^{(0)}(y_c, r_b)$  and  $H_A^{(0)}(y_c, r_b)$  become identical

$$H_V^{(0)}(y_c, 0) = H_A^{(0)}(y_c, 0) \equiv A^{(0)}(y_c) .$$

In this case we obtain the known result for the JADE-type algorithms, which is expressed in terms of the function  $A^{(0)}(y_c)$  also given in appendix C<sup>3</sup>.

To see more clearly the size of mass effects we are going to study the following ratio of jet fractions

$$R_3^{bd} \equiv \frac{\Gamma_{3j}^b(y_c)/\Gamma^b}{\Gamma_{3j}^d(y_c)/\Gamma^d} = \left( c_V \frac{H_V^{(0)}(y_c, r_b)}{A^{(0)}(y_c)} + c_A \frac{H_A^{(0)}(y_c, r_b)}{A^{(0)}(y_c)} \right) (1 + 6r_b c_A + O(r_b^2)) , \quad (3.8)$$

where we have defined

$$c_V = \frac{g_V^2}{g_V^2 + g_A^2} , \quad c_A = \frac{g_A^2}{g_V^2 + g_A^2} .$$

In eq. (3.8) we have kept only the lowest order terms in  $\alpha_s$  and  $r_b$ . The last factor is due to the normalization to total rates. This normalization is important from the experimental point of view but also from the theoretical point of view because in these quantities large weak corrections dependent on the top quark mass [23] cancel. Note that, for massless quarks, the ratio  $\Gamma_{3j}^d(y_c)/\Gamma^d$  is independent on the neutral current couplings of the quarks and, therefore, it is the same for up- and down-quarks and given by the function  $A^{(0)}$ . This means that we could equally use the normalization to any other light quark or to the sum of all of them (including also the c-quark if its mass can be neglected).

---

<sup>3</sup>Note that with our normalization  $A^{(0)}(y_c) = \frac{1}{2}A(y_c)$ , with  $A(y_c)$  defined in ref. [20].

### 3.2 Estimate of higher order contributions

All previous results come from a tree-level calculation, however, as commented in the introduction, we do not know what is the value of the mass we should use in the final results since the difference among the pole mass, the running mass at  $\mu = m_b$  or the running mass at  $\mu = m_Z$  are next-order effects in  $\alpha_s$ .

In the case of the inclusive decay rate we have shown that one could account (with very good precision) for higher order corrections by using the running mass at the  $m_Z$  scale in the lowest order calculations. Numerically the effect of running the quark mass from  $m_b$  to  $m_Z$  is very important.

One could also follow a similar approach in the case of jet rates and try to account for the next-order corrections by using the running quark mass at different scales. We will see below that the dependence of  $R_3^{bd}$  on the quark mass is quite strong (for all clustering schemes); using the different masses (e.g.  $m_b$  or  $\bar{m}_b(M_Z)$ ) could amount to almost a factor 2 in the mass effect. This suggests that higher order corrections could be important. Here, however, the situation is quite different, since in the decay rates to jets we have an additional scale given by  $y_c$ ,  $E_c \equiv m_Z \sqrt{y_c}$ , e.g. for  $y_c = 0.01$  we have  $E_c = 9$  GeV and for  $y_c = 0.05$ ,  $E_c = 20$  GeV. Perhaps one can absorb large logarithms,  $\log(m_b/m_Z)$  by using the running coupling and the running mass at the  $\mu = m_Z$  scale, but there will remain logarithms of the resolution parameter,  $\log(y_c)$ . For not very small  $y_c$  one can expect that the tree-level results obtained by using the running mass at the  $m_Z$  scale are a good approximation, however, as we already said, the situation cannot be settled completely until a next-to-leading calculation including mass effects is available.

Another way to estimate higher order effects in  $R_3^{bd}$  is to use the known results for the massless case [24,20,21]

Including higher order corrections the general form of eq. (3.7) is still valid with the change  $H_{V(A)}^{(0)}(y_c, r_b) \rightarrow H_{V(A)}(y_c, r_b)$ . Now we can expand the functions  $H_{V(A)}(y_c, r_b)$  in  $\alpha_s$  and factorize the leading dependence on the quark mass as follows

$$H_{V(A)}(y_c, r_b) = A^{(0)}(y_c) + \frac{\alpha_s}{\pi} A^{(1)}(y_c) + r_b \left( B_{V(A)}^{(0)}(y_c, r_b) + \frac{\alpha_s}{\pi} B_{V(A)}^{(1)}(y_c, r_b) \right) + \dots \quad (3.9)$$

In this equation we already took into account that for massless quarks vector and axial contributions are identical<sup>4</sup>

Then, we can rewrite the ratio  $R_3^{bd}$ , at order  $\alpha_s$ , as follows

$$\begin{aligned} R_3^{bd} = 1 + r_b & \left[ c_V \frac{B_V^{(0)}(y_c, r_b)}{A^{(0)}(y_c)} \left( 1 + \frac{\alpha_s}{\pi} \left( \frac{B_V^{(1)}(y_c, r_b)}{B_V^{(0)}(y_c, r_b)} - \frac{A^{(1)}(y_c)}{A^{(0)}(y_c)} \right) \right) \right. \\ & \left. + c_A \frac{B_A^{(0)}(y_c, r_b)}{A^{(0)}(y_c)} \left( 1 + \frac{\alpha_s}{\pi} \left( \frac{B_A^{(1)}(y_c, r_b)}{B_A^{(0)}(y_c, r_b)} - \frac{A^{(1)}(y_c)}{A^{(0)}(y_c)} \right) \right) \right] \\ & \times \left( 1 + 6r_b \left( c_A \left( 1 + 2 \frac{\alpha_s}{\pi} \log(r_b) \right) - c_V 2 \frac{\alpha_s}{\pi} \right) \right). \end{aligned} \quad (3.10)$$

From the calculations in this paper we know  $B_V^{(0)}(y_c, r_b)$  and  $B_A^{(0)}(y_c, r_b)$ ; the lowest order function for the massless case,  $A^{(0)}(y_c)$ , is also known analytically for JADE-type algorithms, eq. (C.13) and refs. [20,21], and for the DURHAM algorithm [22]. A parameterization of the

<sup>4</sup>This is not completely true at  $O(\alpha_s^2)$  because the triangle anomaly: there are one-loop triangle diagrams contributing to  $Z \rightarrow b\bar{b}g$  with the top and the bottom quarks running in the loop. Since  $m_t \neq m_b$  the anomaly cancellation is not complete. These diagrams contribute to the axial part even for  $m_b = 0$  and lead to a deviation from  $A_V^{(1)}(y_c) = A_A^{(1)}(y_c)$  [25]. This deviation is, however, small [25] and we are not going to consider its effect here.

function  $A^{(1)}(y_c)$  can be found in [20] for the different algorithms<sup>5</sup>. As we already mentioned this function is different for different clustering algorithms. The only unknown functions in eq. (3.10) are  $B_V^{(1)}(y_c, r_b)$  and  $B_A^{(1)}(y_c, r_b)$ , which must be obtained from a complete calculation at order  $\alpha_s^2$  including mass effects (at least at leading order in  $r_b$ ).

Nevertheless, in order to estimate the impact of higher order corrections in our calculation we will assume that  $B_{V,A}^{(1)}(y_c, r_b)/B_{V,A}^{(0)}(y_c, r_b) \ll A^{(1)}(y_c)/A^{(0)}(y_c)$  and take  $A^{(1)}(y_c)/A^{(0)}(y_c)$  from<sup>6</sup> [20, 21]. Of course this does not need to be the case but at least it gives an idea of the size of higher order corrections. We will illustrate the numerical effect of these corrections for  $R_3^{bd}$  in the next subsection. As we will see, the estimated effect of next-order corrections is quite large, therefore in order to obtain the  $b$ -quark mass from these ratios the calculation of the functions  $B_{V,A}^{(1)}(y_c, r_b)$  is mandatory [26].

### 3.3 Numerical results for $R_3^{bd}$ for different clustering algorithms

To complete this section we present the numerical results for  $R_3^{bd}$  calculated with the different jet-clustering algorithms. For the JADE, E and Durham algorithms we obtained the three-jet rate by a numerical integration over the phase-space given by the cuts (see fig. 2). For the EM scheme we used our analytical results which were also employed to cross check the numerical procedure.

In fig. 3 we present the ratio  $R_3^{bd}$ , obtained by using the tree-level expression, eq. (3.8), against  $y_c$  for  $m_b = 5$  GeV and  $m_b = 3$  GeV. We also plot the results given by eq. (3.10) (with  $B_{V,A}^{(1)}(y_c, r_b)/B_{V,A}^{(0)}(y_c, r_b) = 0$ ) for  $m_b = 5$  GeV, which gives an estimate of higher order corrections. For  $y_c < 0.01$  we do not expect the perturbative calculation to be valid.

As we see from the figure, the behaviour of  $R_3^{bd}$  is quite different in the different schemes. The mass effect has a negative sign for all schemes except for the E-algorithm. For  $y_c > 0.05$  the mass effects are at the 4% level for  $m_b = 5$  GeV and at the 2% level for  $m_b = 3$  GeV (when the tree level expression is used). Our estimate of higher order effects, with the inclusion of the next-order effects in  $\alpha_s$  for massless quarks, shifts the curve for  $m_b = 5$  GeV in the direction of the 3 GeV result and amounts to about of 20% to 40% of the difference between the tree-level calculations with the two different masses. For both E and EM schemes we used the higher order results for the E scheme.

For the JADE algorithm we have also plotted in fig. 3 the experimental results for  $R_3^{bd}$  obtained by the DELPHI group [2] on the basis of the data collected in 1990-1991. The experimental errors, due to the limited statistics analyzed, are rather large. However, one can already see the effect of the quark mass. If the  $b$ -quark mass would be zero, one should obtain a ratio  $R_3^{bd}$  constant and equal to 1. It is clearly seen from the figure that for  $y_c < 0.08$  the data are significantly below 1. For larger values of  $y_c$ , the number of events decreases, the errors become too large and the data are consistent with 1. When larger amount of data is analyzed and the experimental error is decreased, it will be very interesting to see if data will exhibit the different signs of the mass effect in  $R_3^{bd}$  (positive for the E scheme and negative for the other schemes) as predicted by our parton level calculations (see fig. 3).

In spite of the fact that the effect of the quark mass in  $R_3^{bd}$  has been seen, it is too early, in our opinion, to extract now the value of the  $b$ -quark mass from the data. As discussed above the higher order corrections to  $R_3^{bd}$  are presumably rather large and should be included in the theoretical calculations. However, it is clear, that once the essential next-to-leading order

<sup>5</sup>With our choice of the normalization  $A^{(1)}(y_c) = B(y_c)/4$ , where  $B(y_c)$  is defined in [20].

<sup>6</sup>For the EM algorithm this function has not yet been computed. To make an estimate of higher order corrections we will use in this case the results for the E algorithm.



Algorithm	$k_V^{(0)}$	$k_V^{(1)}$	$k_V^{(2)}$	$k_A^{(0)}$	$k_A^{(1)}$	$k_A^{(2)}$
EM	-2.72	-14.64	-28.58	-2.61	-13.54	-30.67
JADE	-2.01	-5.19	-13.25	-1.90	-4.13	-15.42
E	4.68	19.04	25.97	4.71	19.81	23.39
DURHAM	-1.69	-4.76	-12.70	-1.65	-4.28	-15.48

Table 2: Results of the tree parameter fits of the functions  $B_{V,A}^{(0)}(y_c, r_b)/A^{(0)}(y_c) = \sum_{n=0}^2 k_{V,A}^{(n)} \log^n y_c$  in the range  $0.01 < y_c < 0.2$

corrections will be available and all LEP data will be included in the analysis, the ratios  $R_3^{bd}$  will certainly allow for a reasonable determination of the  $b$ -quark mass and for a check of its running from  $m_b$  to  $m_Z$ .

To simplify the use of our results we present simple fits to the ratios  $B_{V,A}^{(0)}(y_c, r_b)/A^{(0)}(y_c)$ , which define  $R_3^{bd}$  at lowest order, for the different clustering algorithms. We use the following parameterization:

$$B_{V,A}^{(0)}(y_c, r_b)/A^{(0)}(y_c) = \sum_{n=0}^2 k_{V,A}^{(n)} \log^n y_c, \quad (3.11)$$

and the results of the fits for the range  $0.01 < y_c < 0.2$  are presented in table 2.

In fig. 4 we plot the ratios  $B_{V,A}^{(0)}(y_c, r_b)/A^{(0)}(y_c)$  as a function of  $y_c$  for the different algorithms (dashed lines for  $m_b = 5$  GeV, dotted lines for  $m_b = 3$  GeV and solid curves for the result of our fits). As we see from the figure the remnant mass dependence in these ratios (in the range of masses we are interested in and in the range of  $y_c$  we have considered) is rather small and for actual fits we used the average of the ratios for the two different masses. We see from these figures that such a simple three-parameter fit works reasonably well for all the algorithms.

Concluding this section we would like to make the following remark. In this paper we discuss the  $Z$ -boson decay. In LEP experiments one studies the process  $e^+e^- \rightarrow (Z\gamma^*) \rightarrow b\bar{b}$  and, apart from the resonant  $Z$ -exchange cross section, there are contributions from the pure  $\gamma$ -exchange and from the  $\gamma - Z$ -interference. The non-resonant  $\gamma$ -exchange contribution at the peak is less than 1% for muon production and in the case of  $b$ -quark production there is an additional suppression factor  $Q_b^2 = 1/9$ . In the vicinity of the  $Z$ -peak the interference is also suppressed because it is proportional to  $Q_b(s - m_Z^2)$  ( $\sqrt{s}$  is the  $e^+e^-$  centre of mass energy). We will neglect these terms as they give negligible contributions compared with the uncertainties in higher order QCD corrections to the quantities we are considering.

Obviously, QED initial-state radiation should be taken into account in the real analysis; the cross section for  $b$ -pair production at the  $Z$  resonance can be written as

$$\sigma_{b\bar{b}}(s) = \int \sigma_{b\bar{b}}^0(s') F(s'/s) ds' \quad (3.12)$$

where  $F(s'/s)$  is the well-known QED radiator for the total cross section [27] and, the Born cross section, neglecting pure  $\gamma$  exchange contribution and the  $\gamma - Z$ -interference, has the form

$$\sigma_{b\bar{b}}^0(s) = \frac{12\pi\Gamma_e\Gamma_b}{m_Z^2} \frac{s}{(s - m_Z^2)^2 + m_Z^2\Gamma_Z^2} \quad (3.13)$$

with obvious notation. Note that  $\Gamma_b$  in this expression can be an inclusive width as well as some more exclusive quantity, which takes into account some kinematical restrictions on the final state.

## 4 Angular distribution

If the gluon jet can be identified with enough efficiency, an interesting quantity which is very sensitive to the IR behaviour of the amplitudes is the angular distribution with respect to the angle formed between one of the quark jets and the gluon jet<sup>7</sup>. If  $\vartheta_1$  ( $\vartheta_2$ ) is the angle between the quark (antiquark) and the gluon jets we define  $\vartheta = \min(\vartheta_1, \vartheta_2)$ . We want to obtain the angular distribution with respect to  $\vartheta$ . The starting point is eq. (3.2) where we change variables from one of the  $y_1$  or the  $y_2$  variables to  $\vartheta$ . To do this we take into account that the amplitude is completely symmetric in  $y_1$  and  $y_2$ , therefore we can restrict the integration only to the region  $y_2 > y_1$  and add a factor 2. In that region  $\vartheta = \vartheta_1$ . Therefore to obtain the distribution with respect to  $\vartheta$  it is enough to obtain the distribution with respect to  $\vartheta_1$  but constraining the phase space integration to  $y_2 > y_1$ .

For  $y_2 > y_1$  we can easily express  $y_1$  in terms of  $\cos \vartheta = \cos \vartheta_1$  as follows

$$y_1 = \frac{y_2 (1 - y_2 - \cos \vartheta \sqrt{(1 - y_2)^2 - 4r_b})}{1 + y_2 + \cos \vartheta \sqrt{(1 - y_2)^2 - 4r_b}}. \quad (4.1)$$

Adding the Jacobian of the transformation we find from eq. (3.2) (taking  $\epsilon = 0$  as this quantity is IR convergent)

$$\frac{d\Gamma_{3j}^b}{d\vartheta} = C_b C_g C_F 2 \int dy_2 \theta_{PS} \theta_c \theta(y_2 - y_1) \sin \vartheta \frac{2y_2 \sqrt{(1 - y_2)^2 - 4r_b}}{(1 + y_2 + \cos \vartheta \sqrt{(1 - y_2)^2 - 4r_b})^2} A_{bg}, \quad (4.2)$$

where  $y_1$  is expressed in terms of  $\cos \vartheta$  and  $y_2$  using eq. (4.1).

In order to see how large mass effects are in this angular distribution we define the following ratio of angular distributions:

$$R_{\vartheta}^{bd} = \frac{1}{\Gamma^b} \frac{d\Gamma_{3j}^b}{d\vartheta} \bigg/ \frac{1}{\Gamma^d} \frac{d\Gamma_{3j}^d}{d\vartheta} \quad (4.3)$$

In the case of massless quarks the integration limits in eq. (4.2) can be found analytically for the JADE-type schemes and the result of the integration over  $y_2$  is expressed in terms of logarithms involving  $\vartheta$  and  $y_c$ . We find

$$\frac{1}{\Gamma^d} \frac{d\Gamma_{3j}^d}{d\vartheta} = \frac{\alpha_s}{\pi} f_{\vartheta}(y_c), \quad (4.4)$$

where the function  $f_{\vartheta}(y_c)$  is given analytically in appendix D for the JADE-type schemes and represented in fig. 5 for the JADE-type and the Durham algorithms for different values of  $y_c$  ( $y_c = 0.02$  (solid line),  $y_c = 0.04$  (dashed line)  $y_c = 0.06$  (dotted line) and  $y_c = 0.08$  (dash-dotted line)). We observe a very sharp peak, for both algorithms, in the region of  $90^\circ$ – $100^\circ$  depending on the value of  $y_c$ , for  $y_c = 0.04$  the peak is at about  $92^\circ$  for the JADE-type algorithms and at about  $99^\circ$  for the Durham algorithm. We see that the absolute size of the peak is a factor two larger in the case of the JADE-type algorithms (for the same value of  $y_c$ ) than in the case of the DURHAM scheme. This is due to the difference of phase spaces for two schemes.

---

<sup>7</sup>We thank J. Fuster for suggesting us the study of this observable.

For massive quarks, although the integrations can still be performed analytically in the EM scheme, some of the integration limits are solutions of polynomial equations of the third degree and the analytical result is not especially enlightening. Then, we have computed the ratio  $R_{\vartheta}^{bd}$  by doing the one-dimensional integration in (4.2) numerically.

Numerical results for  $R_{\vartheta}^{bd}$  are presented in fig. 6 for the different algorithms for  $y_c = 0.04$  and for both  $m_b = 5$  GeV (solid line) and for  $m_b = 3$  GeV (dashed line). In all cases we plot the ratios for the interval of angles for which the differential cross section is still sizable (see fig. 5), i.e.  $\vartheta \approx 45^\circ - 120^\circ$  for JADE-type schemes and  $\vartheta \approx 50^\circ - 130^\circ$  for the DURHAM algorithm. For small angles and  $m_b = 5$  GeV the effect can be as large as 10% of the ratio. Note, however, that the angular distribution, fig. 5, drops down rapidly for such small angles. In addition, since the ratio changes very fast in this region the exact size of the effect will depend on the angular resolution achieved at experiment.

As in the case of ratios of three-jet event rates,  $R_3^{bd}$ , the variation of the ratio of angular distributions,  $R_{\vartheta}^{bd}$ , for  $m_b = 5$  GeV and  $m_b = 3$  GeV gives a measure of the size of higher order corrections.

We observe in all the ratios the irregular behaviour in the region where the massless angular distribution peaks. This is due to the fact that in the massive case the position of the peak is slightly shifted with respect to the massless case. The mismatch between the two peaks appears as a discontinuity in the ratio when seen from large scales.

It will be interesting to see if data really follow these patterns for  $R_{\vartheta}^{bd}$ . A preliminary analysis performed by the DELPHI group [28] seems to indicate that, indeed, data do follow these angular distributions, at least qualitatively, and exhibit the variations present in the different algorithms.

## 5 Discussion and conclusions

In this paper we have presented a theoretical study of quark-mass effects in the decay of the  $Z$ -boson into bottom quarks.

First, we have reproduced, with the complete mass dependences, the results for the inclusive decay rate of the  $Z \rightarrow b\bar{b} + \dots$  to order  $\alpha_s$  by adding gluon bremsstrahlung from the  $b$ -quarks to the one-loop corrected decay width of  $Z \rightarrow b\bar{b}$ . Although the sum of the two contributions is finite, each of them is separately IR divergent. We used dimensional continuation to regularize the IR divergences and gave a complete analytical result in arbitrary space-time dimensions for each of the two contributions.

The main contribution of this paper is, however, the analysis of some three-jet observables which are more sensitive to the value of the quark masses.

For a slight modification of the JADE algorithm (the EM algorithm) we have calculated analytically the three-jet decay width of the  $Z$ -boson into  $b$ -quarks as a function of the jet resolution parameter,  $y_c$ , and the  $b$ -quark mass. The answer is rather involved, but can be expressed in terms of elementary functions. Apart from the fact that these analytical calculations are interesting by themselves, they can also be used to test Monte Carlo simulations. For the EM, JADE, E and DURHAM clustering algorithms we have obtained the three-jet decay width by a simple two-dimensional numerical integration. Numerical and analytical results have been compared in the case of the EM scheme.

We discussed quark-mass effects by considering the quantity

$$R_3^{bd} = \frac{\Gamma_{3j}^b(y_c)/\Gamma^b}{\Gamma_{3j}^d(y_c)/\Gamma^d} = 1 + \frac{m_b^2}{m_Z^2} F(m_b, y_c)$$

which has many advantages from both the theoretical and the experimental point of views. In

particular, at lowest order, the function  $F(m_b, y_c)$  is almost independent on the quark mass (for the small values of the mass in which we are interested in) and has absolute values ranging from 10 to 35 (depending on  $y_c$  and on the algorithm), where the larger values are obtained for  $y_c$  of about 0.01.

At the lowest order in  $\alpha_s$ , we do not know what is the exact value of the quark mass that should be used in the above equation since the difference between the different definitions of the  $b$ -quark mass, the pole mass,  $m_b \approx 5$  GeV, or the running mass at the  $m_Z$ -scale,  $\bar{m}_b(m_Z) \approx 3$  GeV, is order  $\alpha_s$ . Therefore, we have presented all results for these two values of the mass and have interpreted the difference as an estimate of higher order corrections. Conversely one can keep the mass fixed and include in  $F(m_b, y_c)$  higher order corrections already known for the massless case. According to these estimates the  $O(\alpha_s)$  corrections can be about 40% of the tree-level mass effect (depending on the clustering scheme), although we cannot exclude even larger corrections.

By using the lowest order result we find that for moderate values of the resolution parameter,  $y_c \approx 0.05$ , the mass effect in the ratio  $R_3^{bd}$  is about 4% if the pole mass value of the  $b$ -quark,  $m_b \approx 5$  GeV, is used, and the effect decreases to 2% if  $m_b = 3$  GeV.

We have compared our predictions for  $R_3^{bd}$  for the JADE algorithm, with the results obtained from the 1990-1991 data by the DELPHI group [2]. Although the errors obtained in the analysis of this limited sample of data are rather large, especially for  $y_c > 0.08$ , one clearly sees that for small values of  $y$ -cut ( $y_c < 0.08$ ) the experimental points are systematically below 1, thus clearly exhibiting the effect of the mass of the quark, as for massless quark  $R_3^{bd} = 1$ . The size of the effect agrees roughly with the predictions. One can expect the reduction of the experimental error by, at least, a factor two when the data collected in 1992 are included in the analysis. Then, mass effects will be more clearly seen and it will be very interesting to see if data follow the different qualitative behaviour of the ratio  $R_3^{bd}$  as a function of  $y_c$  as predicted by the parton model calculations (positive effect for the E scheme and negative mass effect for the other algorithms). However, in order to extract a meaningful value of the  $b$ -quark mass from the data it will be necessary to include next-to-leading order corrections since the leading mass effect we have calculated does not distinguish among the different definitions of the quark mass (pole mass, running mass at the  $m_b$  scale or running mass at the  $m_Z$  scale). We believe that the future analysis of the whole LEP statistics and its comparison with the theoretical predictions for the three-jet ratios, which meet the future experimental precision, will allow for a good determination of the  $b$ -quark mass at the highest energy scale and for a check of its running from  $m_b$  to  $m_Z$ .

The high precision achieved at LEP allows for a good separation of the gluonic and quark jets and a measurement of the angular distribution of the radiated gluon with respect to the quark momenta. This angular distribution has been calculated for massless quarks analytically for the JADE-type schemes and numerically for the DURHAM algorithm. We have studied the mass effects, for the different jet-clustering algorithms, in the quantity

$$R_\vartheta^{bd} = \frac{1}{\Gamma^b} \frac{d\Gamma_{3j}^b}{d\vartheta} \bigg/ \frac{1}{\Gamma^d} \frac{d\Gamma_{3j}^d}{d\vartheta}.$$

We have shown that, for a reasonable value of the resolution parameter,  $y_c = 0.04$ , the mass effects in this ratio can be as large as 10% of the ratio for  $m_b = 5$  GeV (depending on the algorithm, the angle  $\vartheta$  and the angular resolution). The larger values are obtained for small angles where, however, the angular distribution falls down very rapidly. A fit to this ratio can be used to extract the value of the  $b$ -quark mass. It will be interesting to see if data really follow the predictions for the angular distributions and if the mass effects in the ratio of angular distributions are well described by our results.

Concluding, we have raised the question of the possibility of measuring the  $b$ -quark mass at LEP by using three-jet observables. In our opinion, this is a big challenge for both experimentalists and theorists. Clearly, more work has to be done in order the precision of theoretical predictions meet the experimental accuracy, in particular order  $\alpha_s^2$  calculations and studies of hadronization corrections including mass effects will be needed. However, this effort is worth since it will allow for an independent measurement of  $m_b$  at much larger energies where, presumably, non-perturbative effects are negligible.

## Acknowledgements

We would like to thank J. Fuster for his continuous encouragement, for many helpful discussions and for carefully reading the manuscript. G. Rodrigo acknowledges the CERN theory group for its hospitality during the preparation of this work and the Conselleria de Cultura, Educació i Ciència de la Generalitat Valenciana for financial support. This work was supported in part by CICYT, Spain, under grant AEN93-0234.

## A Phase space in $D = 4 - \epsilon$ dimensions

The phase space for  $n$ -particles in the final state in  $D$ -dimensions [18] ( $D = 4 - 2\epsilon$ ) has the following general form

$$d(P S_n) = (2\pi)^D \prod_{i=1,n} \frac{d^{D-1} p_i}{(2\pi)^{D-1} 2E_i} \delta^D \left( q - \sum_{i=1,n} p_i \right) \quad (\text{A.1})$$

$$= (2\pi)^D \prod_{i=1,n} \frac{d^D p_i}{(2\pi)^{D-1} 2E_i} \delta(p_i^2 - m_i^2) \Theta(E_i) \delta^D \left( q - \sum_{i=1,n} p_i \right) . \quad (\text{A.2})$$

Then doing several trivial integrations we have the following phase-space factor for the process  $Z \rightarrow b\bar{b}$

$$P S_2 = \frac{1}{4\pi} \frac{\beta}{2} \frac{\Gamma(1-\epsilon)}{\Gamma(2-2\epsilon)} \left( \frac{\beta^2 m_Z^2}{4\pi} \right)^{-\epsilon} , \quad (\text{A.3})$$

where  $\beta = \sqrt{1 - 4r_b}$  with  $r_b = m_b^2/m_Z^2$ ,

For the case of the decay into three particles,  $Z \rightarrow b\bar{b}g$ , we have

$$d(P S_3) = \frac{m_Z^2}{16(2\pi)^3} \frac{1}{\Gamma(2-2\epsilon)} \left( \frac{m_Z^2}{4\pi} \right)^{-2\epsilon} \theta(h_p) h_p^{-\epsilon} dy_1 dy_2 , \quad (\text{A.4})$$

where the function  $h_p$  which gives a phase-space boundary in terms of variables  $y_1 = 2(p_1 k)/m_Z^2$  and  $y_2 = 2(p_2 k)/m_Z^2$  has the form

$$h_p = y_1 y_2 (1 - y_1 - y_2) - r_b (y_1 + y_2)^2 . \quad (\text{A.5})$$

## B Inclusive decay rate functions

In this section we collect the functions needed in section 2. The relevant form factors are:

$$f_\epsilon = C_F \left( 1 + \frac{1+\beta^2}{2\beta} \log(c) \right) , \quad (\text{B.1})$$

$$f_{Tf} = C_F \frac{1-\beta^2}{2\beta} \log(c) , \quad (\text{B.2})$$

$$\begin{aligned} f_{Af} &= f_\epsilon \log(r_b) + C_F \left[ -2 - \frac{2+\beta^2}{2\beta} \log(c) \right. \\ &\quad \left. + \frac{1+\beta^2}{\beta} \left( \text{Li}_2(c) + \frac{\pi^2}{3} - \frac{1}{4} \log^2(c) + \log(c) \log(1-c) \right) \right] . \end{aligned} \quad (\text{B.3})$$

In the expression for  $f_{Af}$ , the first term, proportional to  $\log(r_b)$ , comes because our election for the term proportional to the divergence. The vector form factor,  $f_{Vf}$  can be written in terms of the other two form factors,

$$f_{Vf} = f_{Af} + f_{Tf} . \quad (\text{B.4})$$

In terms of these form factors the functions  $F_V$  and  $F_A$  that appear in eq. (2.13) are

$$F_V = \beta \left( \frac{(3-\beta^2)}{2} f_{Vf} + \frac{3}{2} f_{Tf} \right) , \quad (\text{B.5})$$

$$F_A = \beta^3 f_{Af} . \quad (\text{B.6})$$

The functions that come from real bremsstrahlung can be written as follows,

$$G_V = \beta \left( \frac{1}{2}(3 - \beta^2)G_P + G_{Vh} \right) , \quad (\text{B.7})$$

$$G_A = \beta \left( \beta^2 G_P + G_{Ah} \right) , \quad (\text{B.8})$$

where

$$G_P = G_{Ph} + 2f_\epsilon(1 + \log(\beta)) . \quad (\text{B.9})$$

The terms proportional to  $f_\epsilon$  come again from our choice of the coefficient of the divergence, and  $G_{Ph}$  is the finite part coming from the integration of the term proportional to  $h_p$  in the amplitude

$$G_{Ph} = \frac{C_F}{2\beta} \int_c^{1/c} dz g(z) \frac{1+z}{z} \log(g(z)^3 z(1+z)) . \quad (\text{B.10})$$

The result of the integration gives

$$\begin{aligned} G_{Ph} = C_F \left[ -2 \log \left( \frac{4\beta^3}{1-\beta^2} \right) + 2 - \frac{2+\beta^2}{\beta} \log(c) \right. \\ \left. - \frac{1+\beta^2}{\beta} \left( \frac{1}{4} \log^2(c) + \frac{\pi^2}{3} - \text{Li}_2(c) - \text{Li}_2(c^2) - 3 \log(c) \log(1+c) \right) \right] . \end{aligned} \quad (\text{B.11})$$

The functions  $G_{Vh}$  and  $G_{Ah}$  come from the integration of the  $h_V$  and  $h_A$  terms respectively

$$G_{Vh} = \frac{C_F}{4\beta} \int_c^{1/c} dz g(z)^2 \left( z + \frac{1}{z} \right) = -\frac{C_F}{8} \left( 9 + \beta^2 + \frac{9 - 2\beta^2 + \beta^4}{2\beta} \log(c) \right) , \quad (\text{B.12})$$

and

$$G_{Ah} = \frac{1}{2}(3 - \beta^2)G_{Vh} + (1 - \beta^2)\tilde{G}_{Ah} , \quad (\text{B.13})$$

where

$$\tilde{G}_{Ah} = \frac{C_F}{4\beta} \int_c^{1/c} dz g(z)^2 = \frac{C_F}{8} \left( 3 - \beta^2 + \frac{3 - 2\beta^2 - \beta^4}{2\beta} \log(c) \right) . \quad (\text{B.14})$$

## C Three-jet event rate functions

The functions  $H_V^{(0)}$  and  $H_A^{(0)}$ , which give the leading contribution to the three-jet decay rate in the EM algorithm, can be written in the following form

$$\begin{aligned} H_V^{(0)}(y_c, r_b) &= C_F \sum_{i=1,3} \theta_i \left[ \frac{(3 - \beta^2)}{2} K_S^i + K_V^i \right] \\ H_A^{(0)}(y_c, r_b) &= C_F \sum_{i=1,3} \theta_i \left[ \beta^2 K_S^i + \frac{(3 - \beta^2)}{2} K_V^i + (1 - \beta^2) K_A^i \right] . \end{aligned} \quad (\text{C.1})$$

with

$$\begin{aligned} \theta_1 &= \theta(\bar{y}_c - y_c) \\ \theta_2 &= -\theta(y_c - 2r_b)\theta(\bar{y}_c - y_c) \\ \theta_3 &= \theta(y_c - \bar{y}_c) \end{aligned}$$

and  $\bar{y}_c \approx \sqrt{r_b}(1 - \sqrt{r_b})$ . Here  $K_S^i$  corresponds to the soft part and  $K_{V(A)}^i$  to the vector (axial) hard part. These functions are given by

$$\begin{aligned}
K_S^1 &= 4y_c(z_\beta^{-1} - 1) - 2 \left( \frac{1 - \beta^2}{2} + 2y_c \right) \log(z_\beta) + 4\beta \log \left( \frac{z_\beta - c}{1 - z_\beta c} \right) \\
&+ (1 - \beta^2) \left[ 1 + z_\beta^{-1} - 2z_\beta + (z_\beta^{-1} - z_\beta) \log \left( \frac{y_c(1 + z_\beta)(1 + c)^2}{(z_\beta - c)(1 - z_\beta c)} \right) \right] \\
&+ 2(1 + \beta^2) \left[ \frac{1}{2} \log(z_\beta) \log \left( \frac{y_c^2(1 + c)^4}{z_\beta} \right) - \frac{\pi^2}{12} - \text{Li}_2(-z_\beta) - \text{Li}_2 \left( \frac{c}{z_\beta} \right) + \text{Li}_2(z_\beta c) \right]
\end{aligned} \tag{C.2}$$

$$\begin{aligned}
K_V^1 &= 1 + \frac{y_c^2(1 - z_\beta^{-2})}{2} - 2(1 + z_\beta)^{-1} + \frac{(1 - \beta^2)(3 + \beta^2)}{8}(z_\beta - z_\beta^{-1}) \\
&+ \frac{(1 - \beta^2)^2}{32}(z_\beta^{-2} - z_\beta^2) - \left( 1 + \frac{(1 - \beta^2)^2}{8} - y_c^2 \right) \log(z_\beta)
\end{aligned} \tag{C.3}$$

$$\begin{aligned}
K_A^1 &= -\frac{1}{2} + y_c^2(1 - z_\beta^{-1}) + \frac{(1 - \beta^2)^2}{16}(z_\beta^{-1} - z_\beta) + (1 + z_\beta)^{-1} \\
&+ \frac{(1 - \beta^2)(3 + \beta^2)}{8} \log(z_\beta)
\end{aligned} \tag{C.4}$$

$$\begin{aligned}
K_S^2 &= -2(1 + \beta^2 - 2y_c) \log(z_\alpha) + 4\beta \log \left( \frac{z_\alpha - c}{1 - z_\alpha c} \right) \\
&+ (1 - \beta^2)(z_\alpha^{-1} - z_\alpha) \left[ 2 + \log \left( \frac{(1 + \beta^2 - 2y_c)z_\alpha(1 + c)^2}{2(z_\alpha - c)(1 - cz_\alpha)} \right) \right] \\
&+ 2(1 + \beta^2) \left[ \log(z_\alpha) \log \left( \frac{(1 + \beta^2 - 2y_c)(1 + c)^2}{2} \right) - \text{Li}_2 \left( \frac{c}{z_\alpha} \right) + \text{Li}_2(cz_\alpha) \right]
\end{aligned} \tag{C.5}$$

$$\begin{aligned}
K_V^2 &= -(1 + \beta^2 - y_c)y_c \frac{(1 - z_\alpha)}{(1 + z_\alpha)} + \frac{(1 - \beta^2)^2}{32}(z_\alpha^{-2} - z_\alpha^2) \\
&+ \frac{(1 - \beta^2)(3 + \beta^2)}{8}(2 - z_\alpha^{-1} + z_\alpha - 4(1 + z_\alpha)^{-1}) \\
&- \left( \frac{(1 - \beta^2)(7 + \beta^2)}{8} + y_c + \beta^2 y_c - y_c^2 \right) \log(z_\alpha)
\end{aligned} \tag{C.6}$$

$$\begin{aligned}
K_A^2 &= \frac{(1 - \beta^2)^2}{16}(z_\alpha^{-1} - z_\alpha) + \frac{(1 + \beta^2 - y_c)y_c}{2} \frac{(1 - z_\alpha)}{(1 + z_\alpha)} \\
&+ \frac{(1 - \beta^2)(3 + \beta^2)}{8}(-1 + 2(1 + z_\alpha)^{-1} + \log(z_\alpha))
\end{aligned} \tag{C.7}$$



$$\begin{aligned}
K_S^3 &= -\frac{(1+\beta^2)\pi^2}{6} - \frac{(1-\beta^2-4\beta^2 z_\gamma)}{z_\gamma} \frac{(1-z_\gamma)}{(1+2z_\gamma)} + \frac{(1+3\beta^2-2(1-\beta^2)z_\gamma)}{(1+2z_\gamma)} \log(z_\gamma) \\
&+ (1+\beta^2) \left[ \log^2 \left( \frac{z_\gamma}{1+z_\gamma} \right) + 2\text{Li}_2 \left( \frac{z_\gamma}{1+z_\gamma} \right) \right]
\end{aligned} \tag{C.8}$$

$$K_V^3 = \frac{(1+\beta^2)^2}{8} \left( -\frac{3(1-z_\gamma^2)}{(1+2z_\gamma)^2} - \frac{2}{(1+2z_\gamma)} \log(z_\gamma) \right) \tag{C.9}$$

$$K_A^3 = \frac{(1+\beta^2)^2}{8} \left( \frac{1-z_\gamma}{1+2z_\gamma} \right)^2, \tag{C.10}$$

where we used the following notation,

$$\begin{aligned}
z_\alpha &= \frac{1}{2r_b} \left( y_c - \sqrt{y_c^2 - 4r_b^2} \right), \\
z_\beta &= \frac{1}{2r_b} \left( 1 - y_c - 2r_b - \sqrt{(1-y_c)^2 - 4r_b^2} \right), \\
z_\gamma &= \frac{y_c}{1-2r_b-2y_c}, \\
c &= \frac{1-\beta}{1+\beta}.
\end{aligned} \tag{C.11}$$

In the limit of massless quarks,  $r_b \rightarrow 0$ , from the functions  $H_V^{(0)}$  and  $H_A^{(0)}$  given above we obtain

$$H_V^{(0)}(y_c, r_b \rightarrow 0) = H_A^{(0)}(y_c, r_b \rightarrow 0) \rightarrow A^{(0)}, \tag{C.12}$$

Here the function  $A^{(0)}(y_c)$  is the known result [20,21] for the JADE algorithm

$$\begin{aligned}
A^{(0)}(y_c) &= 2C_F \left[ -\frac{\pi^2}{3} + \frac{5}{2} - 6y_c - \frac{9}{2}y_c^2 + (3-6y_c) \log \left( \frac{y_c}{1-2y_c} \right) \right. \\
&\quad \left. + 2 \log^2 \left( \frac{y_c}{1-y_c} \right) + 4\text{Li}_2 \left( \frac{y_c}{1-y_c} \right) \right].
\end{aligned} \tag{C.13}$$

The function  $A(y_c)$  given in refs. [20,21] differs from our  $A^{(0)}(y_c)$  in a factor 2 because we chose a different normalization for it.

## D Angular distribution functions

The angular distribution studied in section 4 is given, in the massless case, by the function  $f_\vartheta(y_c)$ . In the JADE-type algorithms it can be written as follows

$$f_\vartheta(y_c) = C_F \sin(\vartheta) \sum_{i=1,2} \theta_i f_i(y_c), \tag{D.1}$$

where the  $\theta_i$  functions have the form

$$\begin{aligned}
\theta_1 &= \theta \left( \cos \vartheta + \frac{y_c}{(1-y_c)} \right) \theta \left( \frac{(1-6y_c+y_c^2)}{(1+y_c)^2} - \cos \vartheta \right), \\
\theta_2 &= \theta \left( -\frac{y_c}{(1-y_c)} - \cos \vartheta \right) \theta \left( \cos \vartheta + \frac{1-y_c}{1+y_c} \right),
\end{aligned}$$

and

$$\begin{aligned}
f_1(y_c) &= \frac{(1+b)^2}{b} \left[ \frac{y_c + 8b - 3}{4} \sqrt{(1-y_c)^2 - 4by_c} \right. \\
&\quad \left. - \log \left( \frac{x_1}{x_2} \right) + (1+b+2b^2) \log \left( \frac{b+x_1}{b+x_2} \right) \right] , \tag{D.2}
\end{aligned}$$

$$\begin{aligned}
f_2(y_c) &= \frac{(1+b)^2}{b} \left[ \frac{(y_c-b)(y_c^2 + 2y_c - 2by_c - 5b^2)}{4(b+y_c)} \right. \\
&\quad \left. - b(1+2b) \log \left( \frac{2b}{b+y_c} \right) - \log \left( \frac{1-b}{1-y_c} \right) \right] . \tag{D.3}
\end{aligned}$$

In these equations we defined

$$\begin{aligned}
b &= \frac{1 + \cos \vartheta}{1 - \cos \vartheta} , \\
x_1 &= \frac{1}{2} \left( 1 - y_c - \sqrt{(1-y_c)^2 - 4by_c} \right) , \\
x_2 &= \frac{1}{2} \left( 1 - y_c + \sqrt{(1-y_c)^2 - 4by_c} \right) .
\end{aligned}$$

# References

- [1] L3 Collaboration, B. Adeva, et al. , Phys. Lett. **B271** (1991) 461.
- [2] DELPHI Collaboration, P. Abreu, et al., Phys. Lett. **B307** (1993) 221.
- [3] OPAL Collaboration, R. Akers, et al., Z. für Physik C60 (1993) 397.
- [4] ALEPH Collaboration, “Test of flavour independence of the strong coupling constant”, Submitted to Glasgow Conference, 1994, ICHEP94, Ref. 0527.
- [5] J. Chrin, Proc. of the 28th Rencontre de Moriond, Les Arcs, Savoie, France, March 1993, pag. 313, ed. J. Trän Thanh Van.
- [6] J.A. Valls, “Determinación de la constante de acoplamiento fuerte para quarks  $b$ ,  $\alpha_s^b(M_Z)$ , con el detector DELPHI en LEP”, PhD. Thesis, Universitat de València, 1994.
- [7] See for example, P. Langacker and N. Polonsky, Phys.Rev. **D49** (1994) 1454, and references therein.
- [8] For a review see: L.J. Reinders, H. Rubinstein and S. Yazaki, Phys. Rep. **127** (1985) 1. J.H. Kuhn and P. M. Zerwas , Phys. Rep. **167** (1988) 321.
- [9] M.Shifman, A.I. Vainshtein, M.B. Voloshin and V.I. Zakharov Phys. Lett. **77B** (1978) 80; L.J. Reinders, H. Rubinstein and S. Yazaki, Phys. Lett. **103B** (1981) 63; T.H. Chang, K.J.F. Gaemers and W.L. van Neerven, Nucl. Phys. **B202** (1982) 407.
- [10] J. Schwinger, “Particles, Sources and Fields” (Addison-Wesley, Reading, Mass. 1973).
- [11] K.G. Chetyrkin and J.H. Kühn, Phys. Lett. **B248** (1990) 359.
- [12] K.G. Chetyrkin and A. Kwiatkowski, Phys. Lett. **B305** (1993) 285.
- [13] B.L. Ioffe, Phys. Lett. **78B** (1978) 277.
- [14] T.G. Rizzo, Phys. Rev. **D22** (1980) 2213; H.P. Nilles, Phys. Rev. Lett. **45** (1980) 319.
- [15] J. Jersák, E. Laermann and P.M. Zerwas, Phys. Rev. **D25** (1982) 1218; Erratum, Phys. Rev. **D36** (1987) 310.
- [16] A. Ballestrero, E. Maina, S. Moretti, Nucl. Phys. **B415** (1994) 265; A. Ballestrero, E. Maina, S. Moretti, Phys.Lett **B294** (1992) 425.
- [17] JADE Collaboration, W. Bartels et al., Z. für Physik **C33** (1986) 23.
- [18] R. Gastmans and R. Meuldermans, Nucl. Phys. **B63** (1973) 277; W.J. Marciano and A. Sirlin, Nucl. Phys. **B88** 1975 86; W.J. Marciano, Phys. Rev. **D12** (1975) 3861.
- [19] G. Sterman and S. Weinberg, Phys. Rev. Lett. **39** (1977) 1436.
- [20] S. Bethke et al., Nucl. Phys. **B370** (1992) 310.
- [21] Z. Kunszt , P. Nason, G. Marchesini and B.R. Webber, “Z Physics at LEP 1”, Vol 3: “Event Generators and Software”, CERN Yellow Report 89-08 (1989).

- [22] S. Catani et al. Phys. Lett. **B269** (1991) 432; N. Brown and W.J. Stirling, Z. Phys. **C53** (1992) 629.
- [23] A.A. Akhundov, D.Y. Bardin and T. Riemann, Nucl. Phys. **B276** (1986) 1; J. Bernab  u, A. Pich and A. Santamaria, Phys. Lett. **B200** (1988) 569; Nucl. Phys. **B363** (1991) 326; W. Beenakker and W. Hollik, Z. Phys. **C40** (1988) 141.
- [24] R.K. Ellis, D.A. Ross and A.E. Terrano, Nucl.Phys. **B178** (1981) 421; J.G. K  rner and G.A. Schuler, Z. Phys. **26** (1985) 559; G. Kramer and B. Lampe, Z. Phys. **C34** (1987) 497; G.A. Schuler and J.G. K  rner, Nucl.Phys. **B325** (1989) 557.
- [25] K. Hagiwara, T. Kuruma and Y. Yamada, Nucl. Phys. **B358** (1991) 80.
- [26] M. Bilenky, G. Rodrigo and A. Santamaria, work in progress.
- [27] F.A. Berends, G. Burgers and W.L. van Neerven, Nucl. Phys. **B297** (1988) 429; Erratum, Nucl. Phys. **B304** (1988) 921.
- [28] J. Fuster private communication.

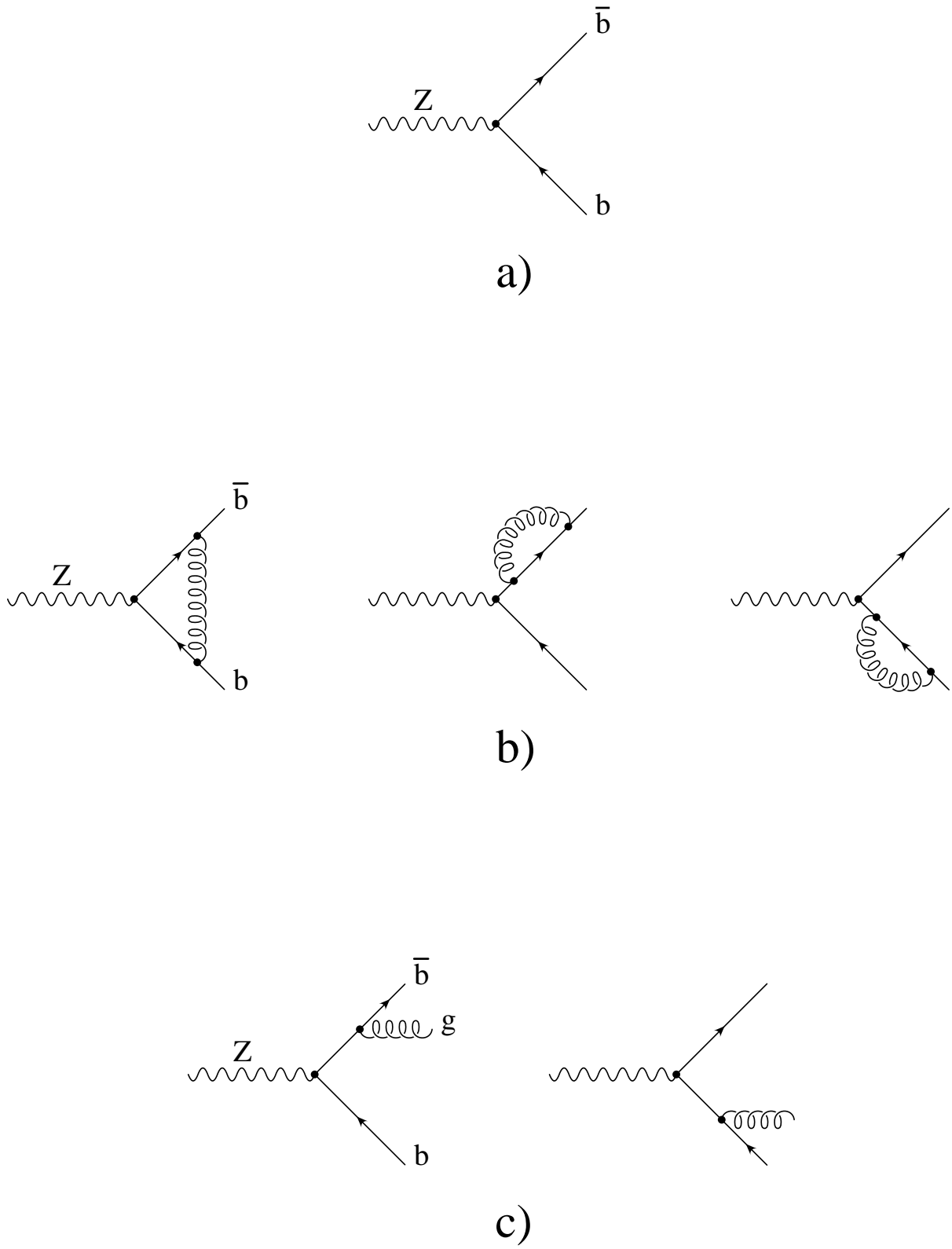


Figure 1: Feynman diagrams contributing to the decay rates  $Z \rightarrow b\bar{b}$ ,  $Z \rightarrow b\bar{b}g$  at order  $\alpha_s$ .

## The phase-space for $Z \rightarrow q\bar{q}g$

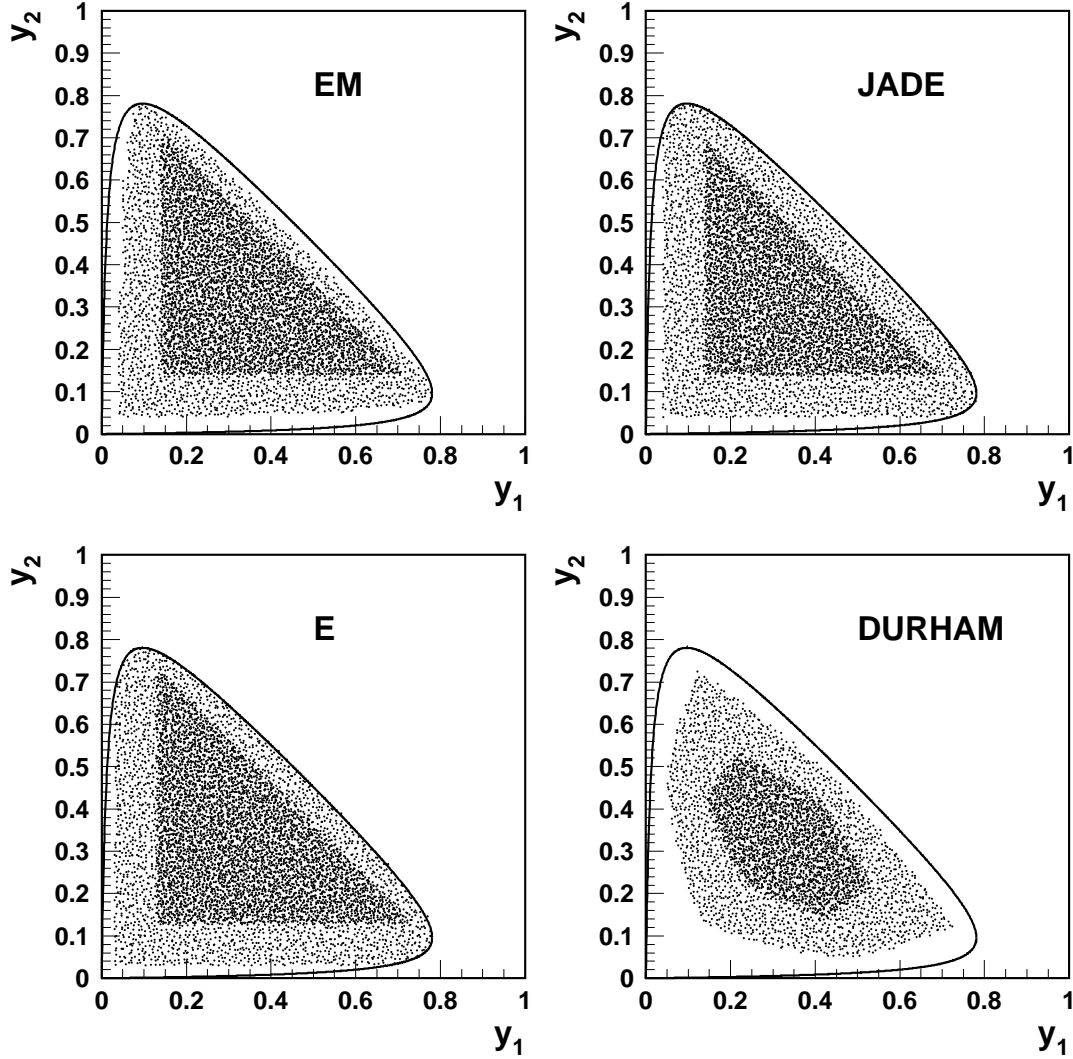


Figure 2: The phase space for  $Z \rightarrow b\bar{b}g$  in the plane  $y_1$  and  $y_2$  with cuts ( $y_c = 0.04$  and  $y_c = 0.14$ ) for the different algorithms. The mass of the quark has been set to 10 GeV to enhance mass effects in the plot.

## The ratios $R_3^{bd}$

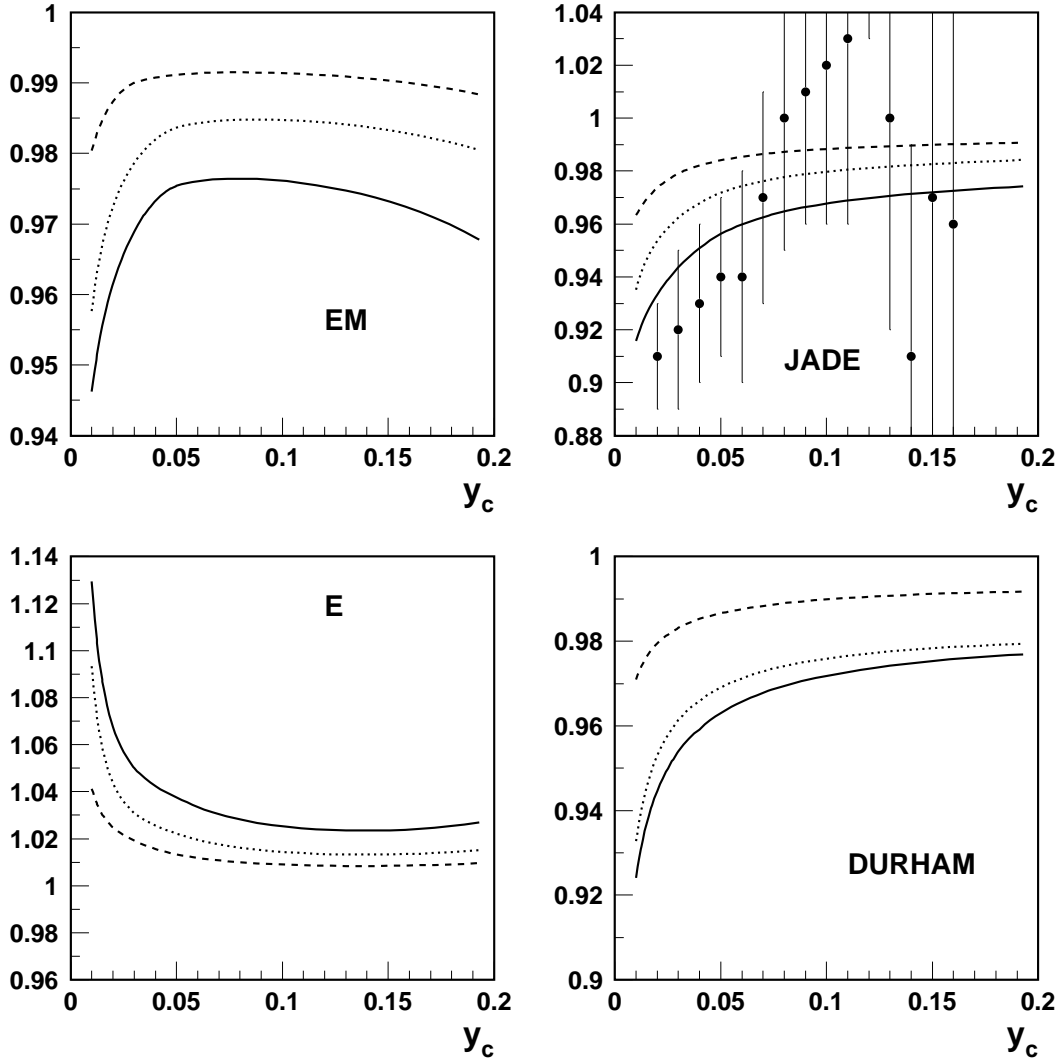


Figure 3: The ratios  $R_3^{bd}$  (see eq. (3.8)) for the four algorithms. Solid lines correspond to  $m_b = 5$  GeV, dashed lines correspond to  $m_b = 3$  GeV and dotted lines give our estimate of higher order corrections to the  $m_b = 5$  GeV curve. For the JADE algorithm we have also included the results of the analysis of the data collected during 1990-1991 by the DELPHI group [2].

## The functions $B_V^{(0)}/A^{(0)}$ and $B_A^{(0)}/A^{(0)}$

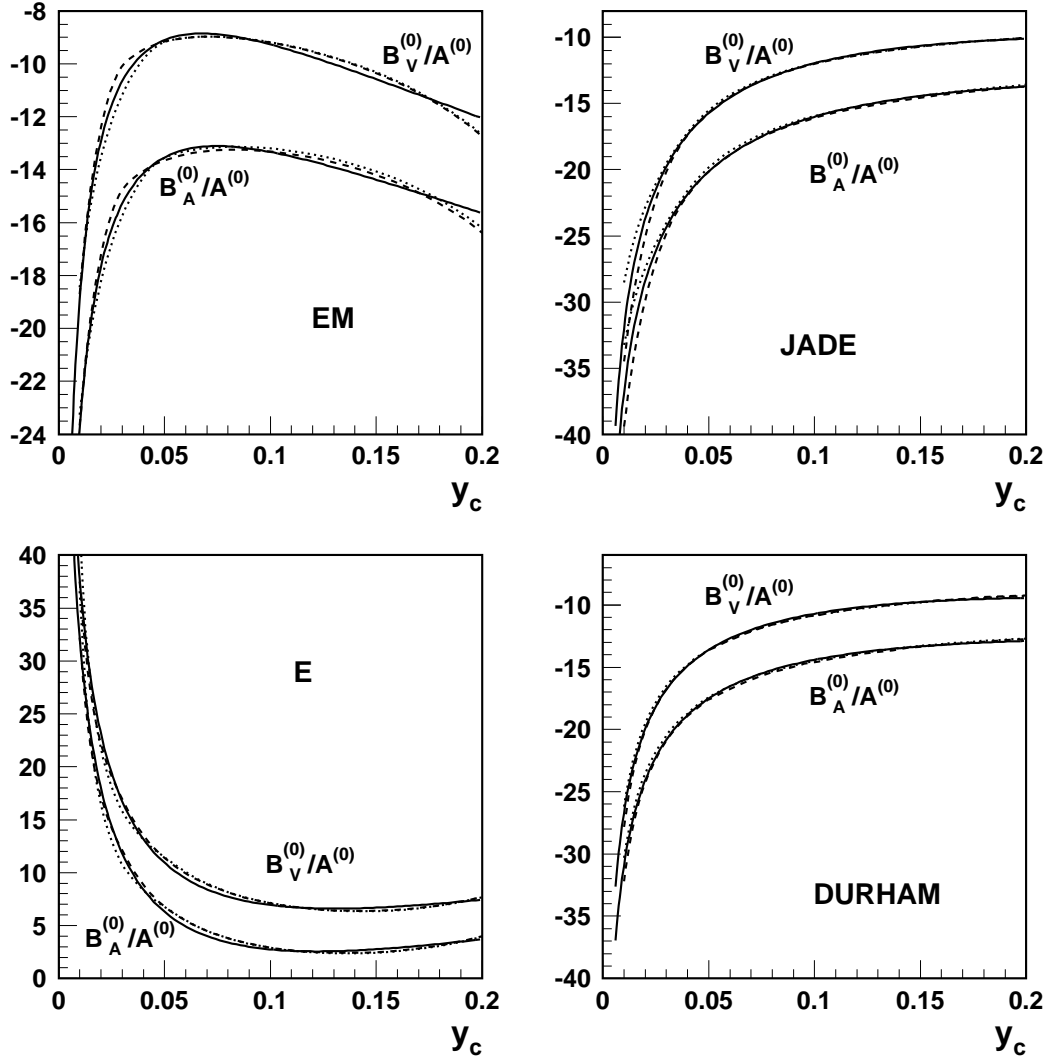


Figure 4: The functions  $B_V^{(0)}/A^{(0)}$  and  $B_A^{(0)}/A^{(0)}$  for the four algorithms. Dashed lines for  $m_b = 3$  GeV, dotted lines for  $m_b = 5$  GeV and solid lines for our three-parameter fit, eq. (3.11).



## Angular distribution ( $m_q=0$ )

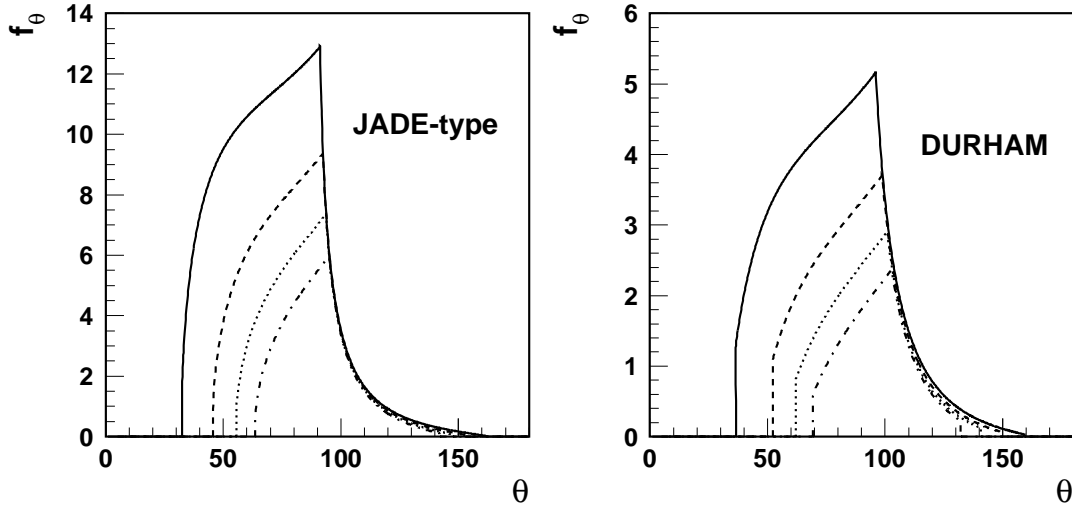


Figure 5: Normalized angular distributions (eq. (4.4)) with respect to the angle formed between the quark and the gluon jets for the massless case for JADE-type and DURHAM algorithms. Solid line for  $y_c = 0.02$ , dashed line for  $y_c = 0.04$ , dotted line for  $y_c = 0.06$  and dash-dotted line for  $y_c = 0.08$

## The ratios $R_{\theta}^{bd}$ ( $y_c = 0.04$ )

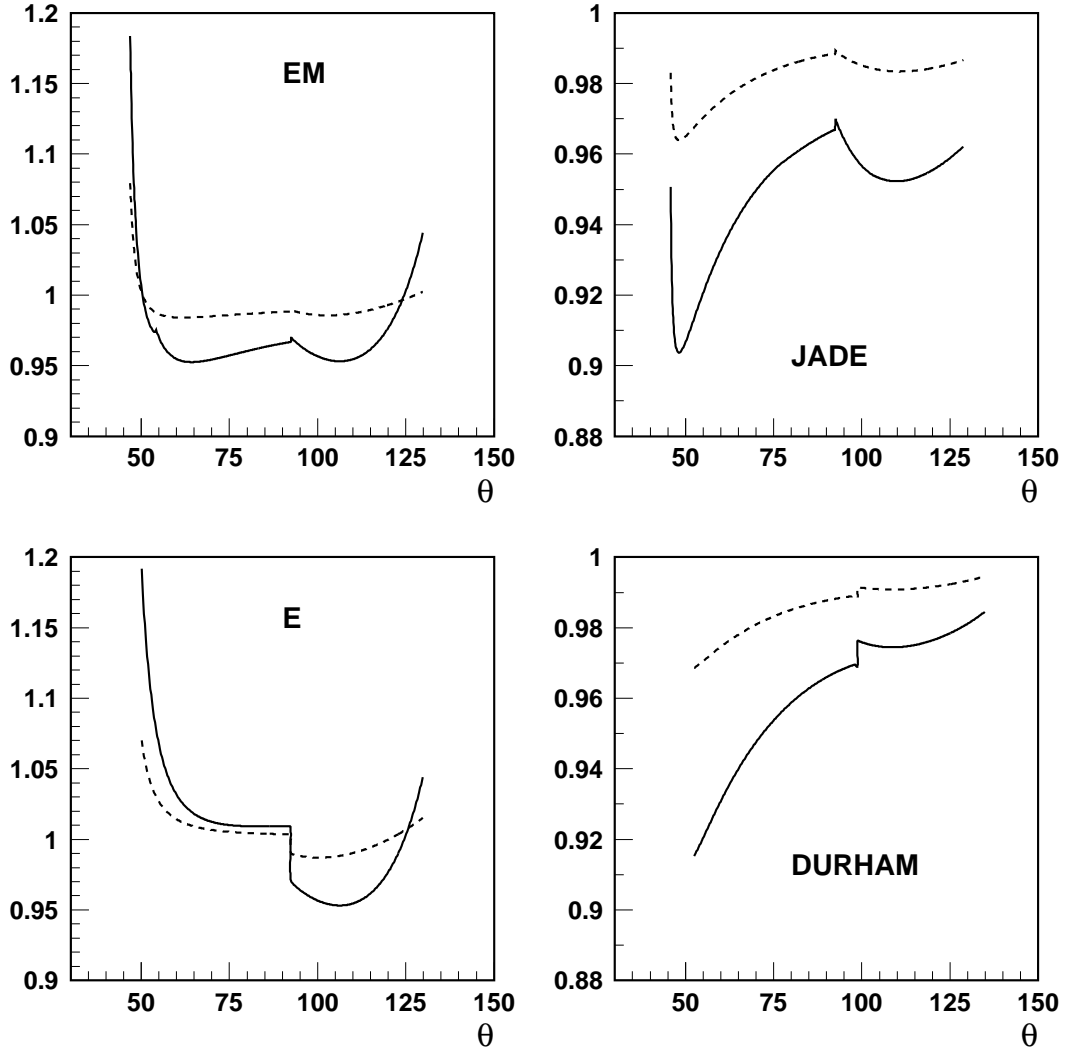


Figure 6: The ratios of angular distributions  $R_{\theta}^{bd}$  (see eq. (4.3)) for  $y_c = 0.04$  for the different algorithms. Solid line for  $m_b = 5$  GeV and dashed line for  $m_b = 3$  GeV.